AFOSR-TR- 81-0863

LEVEL

10

AD A109087

DTIC

DEC 30 1981

H

DTIC FILE COPY

SYSTEMS RESEARCH LABORATORIES INC.

Approved for public release;
distribution unlimited.

81 12 29 034

2800 INDIAN RIPPLE RD. DAYTON, OHIO 45440-3696 (513) 426-6000

UNCLASSIFIED

SECURITY CLASSIFICATION OF THIS PAGE (When Data Entered)

REPORT DOCUMENTATION PAGE		READ INSTRUCTIONS BEFORE COMPLETING FORM
1. REPORT NUMBER **AFOSR-TR- 81 -0863**	2. GOVT ACCESSION NO. AD-A109 087	3. RECIPIENT'S CATALOG NUMBER
4. TITLE (and Subtitle) SURFACE-STRENGTHENING MECHANISMS IN REACTION-BONDED Si_3N_4 AND SUBCRITICAL-CRACK-GROWTH BEHAVIOR IN CERAMICS		5. TYPE OF REPORT & PERIOD COVERED Final Scientific Report 1 Aug 1977 - 30 Sept 1981 6. PERFORMING ORG. REPORT NUMBER 6956 Final
7. AUTHOR(s) M. G. Mendiratta		8. CONTRACT OR GRANT NUMBER(s) F49620-77-C-0124
9. PERFORMING ORGANIZATION NAME AND ADDRESS Systems Research Laboratories, Inc. 2800 Indian Ripple Road Dayton, OH 45440		10. PROGRAM ELEMENT, PROJECT, TASK AREA & WORK UNIT NUMBERS 2306/A2 61102F
11. CONTROLLING OFFICE NAME AND ADDRESS Air Force Office of Scientific Research/NE Bolling Air Force Base Washington, D. C. 20332		12. REPORT DATE November 1981 13. NUMBER OF PAGES 78
14. MONITORING AGENCY NAME & ADDRESS(if different from Controlling Office)		15. SECURITY CLASS. (of this report) Unclassified 15a. DECLASSIFICATION/DOWNGRADING SCHEDULE

16. DISTRIBUTION STATEMENT (of this Report)

APPROVED FOR PUBLIC RELEASE: DISTRIBUTION UNLIMITED

17. DISTRIBUTION STATEMENT (of the abstract entered in Block 20, if different from Report)

18. SUPPLEMENTARY NOTES

19. KEY WORDS (Continue on reverse side if necessary and identify by block number)

Reaction-bonded and hot-pressed silicon nitride, oxidation, chemical vapor deposition, controlled nucleation thermochemical deposition, subcritical crack growth, lithium-aluminum-silicate glass-ceramic, flexural strength

20. ABSTRACT (Continue on reverse side if necessary and identify by block number)

Reported herein are results of a number of investigations on: 1) strength and fracture toughness of oxidized, reaction-bonded (RB) Si_3N_4, 2) evaluation of chemical-vapor-deposition (CVD)-coated reaction-bonded Si_3N_4 and characterization and properties of controlled-nucleation-thermochemical-deposited (CNTD) silicon carbide, 3) subcritical-crack-growth (SCG) behavior of hot-pressed (HP) Si_3N_4 under mixed-mode loading conditions and SCG behavior of oxidized HP Si_3N_4 , and 4) SCG behavior of Lithium-Aluminum-Silicate (LAS)

DD FORM 1 JAN 73 1473 EDITION OF 1 NOV 65 IS OBSOLETE

UNCLASSIFIED

SECURITY CLASSIFICATION OF THIS PAGE (When Data Entered)

Uncl

20. Abstract (Continued)

glass-ceramics. The oxidation of RB Si_3N_4 at 900°C increases the strength by as much as 25%, presumably by blunting the flaw tips associated with open surface pores. The increase in fracture toughness is approximately the same. The 1500°C oxidation, on the other hand, does not provide effective flaw blunting and, in addition, an external silica scale is formed which cracks during cooling. At intermediate temperatures, the post-oxidation strength behavior is intermediate. The CVD-coated RB Si_3N_4 exhibited a significant loss of strength, even though a uniform, adherent coating was produced. The strength of HP Si_3N_4 under mixed-mode loading conditions indicated that the effect of the shear component of applied stress is minimal and that the SCG mainly occurs in Mode I. The pre-oxidation of HP Si_3N_4 decreased the SCG kinetics measurably, presumably due to the depletion of Ca and Mg from the glassy intergranular phase. The SCG behavior of LAS glass-ceramic also indicated that Mode I is the predominant mode of SCG, even in the presence of Modes II and III.

Uncl

10

Final Report
on
Contract F49620-77-C-0124
Covering the Period
1 August 1977 - 30 September 1981

SURFACE-STRENGTHENING MECHANISMS IN REACTION-BONDED Si_3N_4 AND SUBCRITICAL CRACK-GROWTH BEHAVIOR IN CERAMICS

Submitted to

Air Force Office of Scientific Research
Attn: Captain Steve Wax (AFOSR/NE)
Bolling Air Force Base
Washington, D. C. 20332

November 1981

Submitted by

Research Applications Division
Systems Research Laboratories, Inc.
2800 Indian Ripple Road
Dayton, OH 45440

409 171

TABLE OF CONTENTS

SECTION		PAGE
1	INTRODUCTION	1
2	SUMMARY OF MAJOR FINDINGS	3
	Surface Strengthening in RB Si_3N_4	3
	Characterization of Bulk CNTD Silicon Carbide	3
	SCG in HP Si_3N_4	4
	SCG in LAS Glass-Ceramic	5
3	PRESENTATIONS/PUBLICATIONS	6
	APPENDIX	A-1

Section 1

INTRODUCTION

Reaction-bonded (RB) and hot-pressed (HP) Si_3N_4 are the leading candidate materials for jet-engine structural applications. Although these materials possess certain attractive properties, their utilization as jet-engine components is undermined by inadequacies in certain other properties. RB Si_3N_4 is plagued by low strength and fracture toughness, while HP Si_3N_4 exhibits subcritical crack growth (SCG) at elevated temperatures. Therefore, it is important to strengthen RB Si_3N_4 and attempt to understand the mechanisms of SCG in HP Si_3N_4.

Under the present AFOSR contract, a four-year effort has been made to investigate the surface-strengthening mechanisms of RB Si_3N_4 and the SCG of HP Si_3N_4, under both Mode I and mixed-mode loading conditions. In addition, certain other related investigations have been carried out. The research areas covered are listed below:

1) Strength and fracture toughness of oxidized RB Si_3N_4,

2) Evaluation of CVD-coated RB Si_3N_4 and characterization and properties of controlled-nucleation-thermochemical-deposited (CNTD) silicon carbide.

3) SCG behavior of HP Si_3N_4 under mixed-mode loading conditions and SCG behavior of oxidized HP Si_3N_4, and

4) SCG behavior of Lithium-Aluminum-Silicate (LAS) glass-ceramic.

The last material in the above list is considered to be a model material which is thought to simulate closely SCG in HP Si_3N_4. The results of the first two areas and the first part of the third area have been included in the SRL annual reports under this contract.

The major findings of each research area are summarized in the present report. Papers pertaining to the first two research areas have already been published or presented, and the appropriate references are given; papers covering the last two research areas which are being submitted for publication are included in the Appendix.

Section 2

SUMMARY OF MAJOR FINDINGS

SURFACE STRENGTHENING IN RB Si_3N_4

For commercial NC-350 RB Si_3N_4, the room-temperature strength can be significantly increased ($\approx$ 25%) by oxidation exposure at 900°C for even as short a time as 10 hr. This strength increase is attributed to an increase in effective fracture energy caused by the formation of a very thin oxide layer which is responsible for flaw-tip blunting. The strength increase is maintained when the material is further exposed up to 1300°C for a short time, i.e., 10 hr. A slight strength degradation occurs for long-time exposure at 1300°C (200 hr). However, considerable loss in strength is exhibited by the material exposed at 1500°C.

The bend bars of NC-350 RB Si_3N_4 were coated with a uniform film of fully dense α-Si_3N_4 utilizing chemical vapor deposition* (CVD). Two different coating thicknesses, 10 and 50 μm, were utilized. While the cross-sectional SEM examination of the coatings revealed good, uniform adhesion, the strength of the coated bars decreased significantly as compared to that of uncoated bars. This strength degradation was thought to be due to the presence of large crystallites (16 - 20 μm) in the coating.

CHARACTERIZATION OF BULK CNTD SILICON CARBIDE

Utilizing the CNTD process, ultrafine-grained SiC was deposited† with superior surface smoothness and without the macro-columnar growth commonly found in conventional CVD material. At both room and high temperature, the CNTD-SiC with as-deposited surfaces exhibited a bend strength of 200,000 psi (1390 MPa) or more. This is significantly higher than for SiC made by

---

*Coatings produced by Chemetal.

†Chemetal.

conventional sintering, hot pressing, or CVD processes. Room-temperature strengths were significantly reduced by abrasion but were still comparable to or greater than the strength of unabraded material produced by conventional processes. Furthermore, while oxidation may have raised the strength of previously abraded rods, it also appeared that the oxide scale might have been the source of critical flaws.

Several factors suggested variable residual tensile stresses of the order of 100,000 psi (690 MPa). The reduction or elimination of this residual tensile stress could correspondingly raise room-temperature strengths.

The excellent retention of strength at high temperatures is attributed to the high purity and fine grain size of the SiC deposit made by the CNTD process. The rates of weight change for CNTD-SiC during oxidation are lower than for NC-203 (hot-pressed SiC), higher than for GE's CVD-SiC, and CVD-Si_3N_4, but considerably below those for hot-pressed Si_3N_4 (HS-130). Since the material was of high purity, was fully dense, and did not exhibit grain growth at elevated temperatures, it should retain its desirable high-temperature properties for long times. The material shows potential for future use; however, some potential problem areas are scaling the process to make larger parts, deposition on removable substrates, and the possible residual tensile stress.

SCG IN HP Si_3N_4

Mixed-mode loading conditions were achieved by orienting the indentation-produced controlled surface flaws at 45 degrees to the applied-bending-tensile-stress axis. In HP Si_3N_4 the microstructural observations of SCG at 1300°C indicated that initially the crack grew in its own plane (i.e., in the 45-degree direction). However, the extent of this growth was very limited, and most of the crack extension occurred perpendicular to the applied stress. The measured average crack velocities for equivalent applied stress were somewhat smaller in the case of the 45-degree flaw than for the 90-degree flaw, the difference being attributed to the initial time expended in the growth of the 45-degree crack in its own plane. Thus, the shear component plays a minor role in decreasing the SCG velocity. These conclusions were drawn from rather limited data, although a large number of experiments were carried out, the reason being the unpredictably fast SCG from the natural flaws which were thought to be "non-critical." This behavior is attributed to local interactions of natural flaws with the chemical and microstructural heterogeneities in the particular HP Si_3N_4 billet.

It was thought that the oxidation of HP Si_3N_4 might decrease the SCG and improve the situation somewhat since during oxidation, Mg and Ca diffuse from the interior of the HP Si_3N_4 to the external silica scale, leaving an Mg- and Ca-depleted zone near the external surface. Reduction of Mg and Ca should increase the viscosity of the grain-boundary glassy phase, thus decreasing the propensity for SCG. Oxidation at 1375°C resulted in a measurable decrease in SCG velocity, despite the presence of oxidation-produced pits. It was concluded, however, that the beneficial effects of oxidation upon the SCG behavior cannot be fully realized unless the formation of pits can be eliminated or minimized.

SCG IN LAS GLASS-CERAMIC

Although the LAS glass-ceramic was chosen on the assumption that it is a "well-behaved" material in terms of chemical and microstructural homogeneity, a significant scatter in the elevated-temperature strength was observed. The fracture toughness, K_{IC}, was measured as a function of temperature; it was found that K_{IC} decreased appreciably above 850°C. This decrease was attributed to intergranular cavity formation. At high temperatures, the SCG proceeds by simultaneous crack healing and blunting, and it was also found that the SCG occurs essentially in the Mode I loading condition, even when other modes are present.

Section 3

PRESENTATIONS/PUBLICATIONS

"Strength and Fracture Toughness of Oxidized Reaction-Bonded Si_3N_4," M. G. Mendiratta and H. C. Graham. Presented at the Third Annual Conference of the Ceramic-Metal Systems Division of the American Ceramic Society, Merritt Island, FL, January 22, 1979. Published in the Bulletin of the American Ceramic Society, Vol. 60, No. 6, pp. 623-625, 628 (1981).

"Characterization and Properties of Controlled Nucleation Thermochemical Deposition (CNTD) - Silicon Carbide," S. Dutta, R. W. Rice, H. C. Graham, and M. G. Mendiratta. Published in the Journal of Materials Science, Vol. 15, pp. 2183-2191 (1980).

"Subcritical-Crack-Growth Behavior in Si_3N_4 under Mixed-Mode Loading Conditions," G. Das and M. G. Mendiratta. Presented at the 82nd Annual Meeting of the American Ceramic Society, Chicago, IL, April 27-30, 1980.

In addition, two papers which have been prepared for publication are included in the Appendix. These papers are being submitted to the Journal of Materials Science.

APPENDIX

MICROSTRUCTURES AND SUBCRITICAL CRACK GROWTH IN OXIDIZED HOT-PRESSED Si_3N_4

G. Das, M. G. Mendiratta, and G. R. Cornish

Systems Research Laboratories, Inc.
2800 Indian Ripple Road
Dayton, OH 45440

The microstructure of the oxide scales--primarily the size, distribution, and density of the pits--was characterized in hot-pressed Si_3N_4 oxidized at different temperatures from 1300 to 1450°C. These microstructural features and the chemical changes in Si_3N_4 due to oxidation were related to the elevated-temperature subcritical-crack-growth (SCG) behavior. Oxidation at 1375°C for 240 hr. resulted in a measurable improvement in SCG over that in as-hot-pressed and 1300°C-oxidized Si_3N_4.

1. Introduction

Many structural ceramics, e.g., hot-pressed (HP) Si_3N_4, SiC, and Al_2O_3, exhibit subcritical-crack-growth (SCG) behavior under load at elevated temperatures [1-5]. SCG can cause structural failure at a stress level significantly below the short-term fracture stress. The propagation of SCG is commonly related to the presence of glassy phases in the grain boundaries of these materials.

It has been observed [6-7] that during oxidation of Si_3N_4 (hot pressed with MgO as a densification aid), Mg and Ca diffuse from the interior of Si_3N_4 to the external silica scale, creating an extensive depletion of Mg and Ca in the bulk. The removal of Mg and Ca which are the elements in the grain-boundary glassy phase reduces the viscosity of the glassy phase; therefore, after oxidation, the propensity for SCG should decrease. In fact, there is some evidence that the bulk creep resistance of HP Si_3N_4 is improved through oxidation [8]. The present paper describes the microstructural observations of oxide layers resulting from oxidation of HP Si_3N_4 at elevated temperatures and the effects of oxidation upon the subsequent SCG behavior under the Mode I loading condition.

2. Experimental Procedure

HP Si_3N_4 (NC-132) bend bars (5.08 × 0.640 × 0.32 cm) used in this study were purchased from Norton Co. For NC-132, MgO was used as a densification aid. The chemical analysis of Si_3N_4 is shown in Table I. The edges of the tensile surface of the bend bars were rounded to reduce edge flaws. The bend bars were polished on the tensile surface in a direction parallel to the specimen length on a 15-μm diamond wheel and then with 6-μm diamond paste prior to oxidation.

Oxidation was carried out at 1300°C for 36 hr., at 1375°C for 240 hr., and at 1450°C for 240 hr. inside the furnace in static air. Following oxidation, the oxide layer was removed in small steps from the tensile side by polishing with 6-μm diamond paste. After each step (removal of ~ 3 μm), the microstructure of the surface was examined by scanning-electron and light microscopy. Several controlled surface microcracks were produced on the tensile surface of the bend bars which had been carefully polished to remove the oxide layer. Nearly semi-circular microcracks of radius ~ 90 μm were produce by a Knoop diamond indentor utilizing a 2.6-kg indentation load. The details of the technique involving the use of controlled flaws in studying the SCG of HP Si_3N_4 have been described in a recent publication [9].

The bend bars containing the controlled cracks were subjected to a predetermined stress of 196 MN/m^2 (28.5 ksi) in a four-point-bend fixture on an Instron at 1300°C in a vacuum of ~ 10^{-5} Torr for various hold times in order to grow the cracks subcritically. It has been shown [9] that significant SCG occurs at the stress and temperature values selected for the present study. The applied stress was perpendicular to the crack plane, creating a Mode I loading condition. The predetermined stress was reached using a cross-head speed of 5×10^{-3} cm/min.; once the desired stress was attained, the cross-head movement was stopped. In most of the experiments, the stress was held at the desired level by manual control until fracture. The surface-crack extensions were measured by light and scanning-electron microscopy. Average crack-growth velocity was calculated by dividing the crack extension by the corresponding hold time.

3. Results

3.1 Microstructures of As-Oxidized Surface Layers

The surface oxide layer in HP Si_3N_4 resulting from oxidation at 1300°C for 36 hr. consists of needle-like and globular crystallites as shown in Fig. 1. Cracks were readily visible in the oxide layers (shown by arrows in Fig. 1). The thickness of the oxide layer as determined from a cross-sectional view was rather nonuniform throughout. An average thickness was determined to be ~ 12 μm. Occasional large pits were observed within the oxide layer (Fig. 2).

The oxide-scale morphology in Si_3N_4 following oxidation at 1375°C for 240 hr. is shown in Fig. 3 to consist of well-developed needle-like crystallites with cracks being present. The thickness of the oxide layer was found to vary throughout the cross section, and an average thickness was determined to be ~ 50 μm.

A significant change in the appearance of the oxide-scale morphology occurred after oxidation at 1450°C for 240 hr. The oxide surface layer appeared glassy and was highly nonuniform with readily observable cracks, as shown in Fig. 4. Visual inspection revealed a glazed appearance in some regions, suggesting that melting of the oxidized layer had occurred during oxidation. Tripp and Graham [10] made a similar observation in their oxidation of Si_3N_4 at 1450°C. In the present experiments, sagging in the middle of the bars was visible after oxidation at 1450°C for 240 hr. Although sagging was also observed after oxidation at 1300 and 1375°C, the relative magnitude is very small compared to that observed for bars oxidized at 1450°C.

Oxidation at 1450°C for 240 hr. resulted in a considerably thicker oxide scale, with large variation throughout the cross section, ranging from 25 to 250 μm.

Electron-microprobe and EDAX examinations were performed on oxidized specimens to determine qualitatively the chemical concentration--especially of Mg and Ca--within the oxidized scale. Electron-mrcroprobe analysis of a cross-section of a specimen oxidized at 1300°C for 36 hr. showed that the concentration of Mg was high in the outer oxide layer and decreased to a constant level at a distance of ~ 100-150 μm from the outer oxide layer. The Ca concentration was very low in the specimen, but a concentration of Ca-rich material was detected in the outer oxide layer (see Fig. 5). Qualitatively, similar observations were made for specimens oxidized at 1375°C for 240 hr. and 1450°C for 240 hr. These observations are in agreement with earlier investigations [7].

EDAX also showed the outer oxidized surface to be rich in Mg and Ca in all oxidized specimens. In addition, small WC particles (presumably introduced during the ball-milling operation) were present in both as-hot-pressed and-oxidized Si_3N_4.

Prior to introduction of the controlled cracks in the oxidized bars, the oxide layer was removed by polishing with 6-μm diamond paste. Figure 6-8 show the microstructures corresponding to the progressive removal of the oxide layers of Si_3N_4 oxidized at 1300°C for 36 hr., 1375°C for 240 hr., and 1450°C for 240., respectively. Pits become visible as material is gradually removed from the oxidized layers. Numerous pits of different sizes are observed in 1300°C-oxidized Si_3N_4 even after the oxidized layer has been completely removed (Fig. 6c). The pit-size distribution in the surface following removal of the oxide layers in 1300°C-oxidized Si_3N_4 is shown in Fig. 9. In general, the population density of pits having dimensions of 5 μm or less was the highest, followed by pits having sizes between 5 and 10 μm. The number of pits having dimensions greater than 10 μm was low, and only a few pits having dimensions greater than 20 μm were observed. On the other hand, pits remaining on the surface after the oxide layer had been removed in 1375°C-oxidized specimens appeared to have a more or less uniform distribution (Fig. 7). Most of them were spherical in shape with an average size of 40 μm. In contrast, the size of the pits observed on the surface following removal of the oxide layer in 1450°C-oxidized specimens was very small compared to those in 1300- and 1375°C-oxidized specimens; however, their density was significantly higher. Occasionally, large pits were also present in the oxide scale (Fig. 8).

3.2. Subcritical Crack Growth

3.2.1. As-Hot-Pressed Si_3N_4

As-hot-pressed Si_3N_4 bars having controlled flaws on the tensile surface were subjected to a stress of 196 MN/m^2 (28.5 ksi) at 1300°C in four-point-bend tests until fracture occurred. It has been observed that time to fracture varied from 7 to 17 min. In all cases, fracture took place away from the controlled flaws at the cracks growing subcritically from the edge of the sample.

SCG from the controlled flaws was observed in all of the above specimens, as shown in Fig. 10. The controlled flaws grew along the initial plane of the indent in a direction perpendicular to the applied load. Crack extension was observed at both ends of the initial indent, the amount of extension being approximately the same. The crack path was rather straight, with some crack branching.

3.2.2. 1300°C-Oxidized and Polished Si_3N_4

Four experiments utilizing these specimens with controlled flaws were tested until fracture occurred, and the time to fracture varied from 5 to 31 min. The location of fracture in the 1300°C-oxidized specimens was found to have undergone a dramatic change as compared to that in the as-hot-pressed Si_3N_4 in that three out of four specimens failed at cracks subcritically growing from the controlled flaws and the fourth specimen failed at the loading pin. An additional specimen was subjected to an identical stress at 1300°C for 30 min. and was unloaded before fracture. This specimen exhibited considerable bending and also SCG from the controlled flaws.

As in case of unoxidized Si_3N_4, the crack grew in a direction perpendicular to the applied load (Fig. 11); however, it deviated from the initial plane of the indent, and the amount of crack extension at each end of the initial indent was different. Considerable crack branching was observed together with cracks emanating from the natural flaws. Frequently, the crack growing from the initial indent was found to disappear at one end of a pit present in the oxidized and polished material and to become visible again at the other end. In addition, a number of cracks subcritically growing from pits was also observed.

3.2.3. 1375°C-Oxidized and Polished Si_3N_4

The time required to fracture was higher for 1375°C-oxidized bars than that for as-hot-pressed and 1300°C-oxidized specimens. It varied from 31.5 to 47 min. All three bars failed from cracks subcritically growing from the controlled flaws. Additionally, the slow-crack-growth behavior was essentially the same as described earlier.

3.2.4. 1450°C-Oxidized and Polished Si_3N_4

These specimens failed at 117 and 172 MN/m^2 before attaining the predetermined stress level of 196 MN/m when tested in four-point bending at 1300°C. However, no evidence for cracks growing subcritically from the controlled flaws was found. It may be speculated that the high density of small pits and occasionally large pits present in the specimen following oxidation at 1450°C act as stress-raisers and lead to catastrophic failure long before the controlled cracks become critical.

Data on time to fracture for as-hot-pressed and oxidized bend bars subjected to a stress of 196 MN/m^2 (28.5 ksi) at 1300°C for different oxidation treatments are plotted in Fig. 12. It appears that oxidation of Si_3N_4 at 1375°C for 240 hr. has led to an improvement over that of the as-hot-pressed and 1300°C-oxidized specimens with regard to retarding slow-crack-growth behavior.

The SCG data are summarized in Table II which includes hold times and approximate ranges of average crack-growth velocity. The crack-growth velocity was found to vary from indent to indent within the same bar. In some cases, such a variation is rather significant.

4. Discussion

Several factors are known to affect SCG behavior in Si_3N_4, including (1) the chemical nature of the grain-boundary glassy phase, (2) microstructural inhomogeneities, (3) chemical inhomogeneities, and (4) surface conditions. From the microprobe results, it is evident that Mg and Ca have diffused from the interior of the oxidized Si_3N_4 to the external oxidized surface. Mg and Ca are the elements in the grain-boundary glassy phase which reduce viscosity at high temperature, and the propensity for SCG should decresase after oxidation. In fact, Lange [8] has observed that the bulk creep resistance of HP Si_3N_4 was improved through oxidation. In hot-pressed β' Si-Al-O-N ceramics, high-temperature creep and SCG properties were also improved by elevated-temperature heat treatments [11].

It has been observed that in as-hot-pressed Si_3N_4 with controlled flaws subjected to four-point-bend tests at 1300°C, fracture always takes place from flaws subcritically growing from the edge. This seems to suggest that chemical and microstructural inhomogeneities in this material are so severe that natural flaws readily become critical before the controlled flaws. However, upon oxidation at 1300°C, the majority of bars failed from cracks growing from the controlled flaws. This situation was further improved upon oxidation at 1375°C when all bend bars failed from cracks growing from the controlled flaws, although cracks growing from natural flaws were also observed. This behavior, coupled with the observations that bend bars oxidized at 1375°C for 240 hr. yielded longer hold times to fracture as compared to those of as-hot-pressed and 1300°C-oxidized specimens, suggests that oxidation at elevated temperatures must result in a modification of the chemical and microstructural heterogeneity in the Si_3N_4 in such a way that the controlled flaws become critical before other natural flaws have the opportunity to do so.

It should be mentioned, however, that although an overall improvement in the SCG behavior was achieved in 1375°C-oxidized Si_3N_4 despite the presence of pits (aver. size ~ 40 μm), the beneficial effects of oxidation upon the SCG behavior cannot be fully realized unless the formation of pits which results from oxidation at elevated temperatures can be eliminated or minimized.

5. Summary and Conclusions

The surface oxide layer in HP Si_3N_4 resulting from oxidation at 1300 and 1375°C in static air consisted of needle-like and globular crystallites. The oxide layer appeared to have undergone melting at 1450°C. Cracks were observed in the surface oxide layers of all specimens.

Pits present in the surface following removal of the oxide layer showed a variation in size, with the density of pits having dimensions of 5 μm or less being the highest at 1300°C. At 1375°C, pits were more or less spherical with an average size of 40 μm. On the other hand, numerous small pits were observed at 1450°C.

Oxidation at 1375°C resulted in a measurable improvement in SCG over that of as-hot-pressed and 1300°C-oxidized Si_3N_4, despite the presence of pits. However, it is believed that the beneficial effects of oxidation upon the SCG behavior cannot be fully realized unless the formation of pits can be eliminated or minimized.

ACKNOWLEDGEMENT

The authors wish to thank B. M. Lipsitt for experimental assistance. This program was supported by U.S. AFOSR Contract F49620-77-C-0124.

References

1. F. F. LANGE, J. Am. Ceram. Soc. 57 (1974) 84.

2. A. G. EVANS, and S. M. WIEDERHORN, J. Mater. Sci. 9 (1974) 270.

3. A. G. EVANS, M. LINZER, and L. R. RUSSELL, Mater. Sci. Eng. 15 (1974) 253.

4. A. G. EVANS, in "Ceramics for High Performance Applications," 1973 Proceedings of the Second Array Materials Technology Conference, edited by J. J. Burke, A. E. Gorum, and R. N. Kate (Brook Hill Publishing Co., Chestnut Hill, MA, 1974) p. 373.

5. K. D. MCHENRY and R. E. TRESSLER, J. Am. Ceram. Soc. 63 (1980) 152.

6. S. C. SINGHAL J. Mater. Sci. 11 (1976) 500.

7. D. CUBICCIOYTI, K. H. LAU, and R. L. JONES, J. Electrochem. Soc. 124 (1977) 1955.

8. F. F. LANGE and B. I. DAVIS, Bull. Am. Ceram. Soc. 59 (1980) 827.

9. M. G. MENDIRATTA and J. J. PETROVIC, J. Am. Ceram. Soc. 61 (1978) 226.

10. W. C. TRIPP and H. C. GRAHAM, J. Am. Ceram. Soc. 59 (1976) 399.

11. B. S. B. KARUNARATNE and M. H. LEWIS, J. Mater. Sci. 15 (1980) 1781.

FIGURE CAPTIONS

FIGURE

1 a. Scanning electron micrograph showing both needle-like and globular crystallities on the surface of HP Si_3N_4 oxidized at 1300°C for 36 hr.

b. Scanning electron micrograph showing mostly globular crystallites on the surface of HP Si_3N_4 oxidized at 1300°C for 36 hr.

2 Scanning electron micrograph showing a large pit in the oxidized layer (cross-sectional view) of HP Si_3N_4 oxidized at 1300°C for 36 hr.

3 Scanning electron micrograph of the surface of HP Si_3N_4 oxidized at 1375°C for 240 hr.

4 Scanning electron micrograph of the surface of HP Si_3N_4 oxidized at 1450°C for 240 hr. Cracks are readily observed.

5 Electron-microprobe scan showing Ca concentration mostly at the outer oxide layer (light areas) in HP Si_3N_4 oxidized at 1300°C for 36 hr. (cross-sectional view).

6 Progressive removal of outer oxidized layer in Si_3N_4 oxidized at 1300°C for 36 hr. (same area).

7 Progressive removal of outer oxidized layer in Si_3N_4 oxidized at 1375°C for 240 hr.

8 Progressive removal of outer oxidized layer in Si_3N_4 oxidized at 1450°C for 240 hr.

9 Pit-size distribution in specimens following removal of oxidized layer in Si_3N_4 oxidized at 1300°C for 36 hr. Total area - 200 μm × 180 μm in each case.

10 Crack extension in as-received Si_3N_4 tested in four-point bending at 1300°C. Applied stress is 196 MN/m^2.

11 Crack extension in 1300°C-oxidized Si_3N_4 tested in four-point bending at 1300°C. Applied stress is 196 MN/m^2.

12 Hold time to fracture for as-hot-pressed, 1300°C-oxidized, and 1375°C-oxidized Si_3N_4 tested in four-point bending at 1300°C. Applied stress is 196 MN/m^2.

Table I

Chemical Analysis of NC-132 Si_3N_4

Element	Weight Percent
Mg	0.83
Al	0.27
Fe	0.47
Ca	0.063
Mn	0.077
B	0.24
W	2

Table II

Subcritical-Crack-Growth Data for HP and Oxidized $Si_3\dot{N}_4$ Tested at 1300°C

Specimen History	Hold Time (Min)	Range of Velocity (μ/sec)	Comments
As-Received & Polished	7	0.45-0.78	Failed due to SCG from edge.
As-Received & Polished	9	0.31-0.58	Failed due to SCG from edge.
As-Received & Polished	13	0.19-1.2	Failed due to SCG from edge.
As-Received & Polished	15	0.55-0.69	Failed due to SCG from edge.
As-Received & Polished	17	0.39-2.97	Failed due to SCG from edge.
Oxidized at 1300°C, 36 hr. and Polished	5	0.48-1.13	Failed due to SCG from a controlled crack.
Oxidized at 1300°C, 36 hr. and Polished	14	0.53-0.73	Failed due to SCG from a controlled crack.
Oxidized at 1300°C, 36 hr. and Polished	20	0.2-0.44	Failed due to SCG from a controlled crack.
Oxidized at 1300°C, 36 hr. and Polished	31	0.39-0.48	Failed due to SCG from edge.
Oxidized at 1300°C, 36 hr. and Polished	30	0.27-0.51	Bent and showed SCG from controlled cracks, but did not break.
Oxidized at 1375°C, 240 hr. and Polished	31.5		Failed due to SCG from a controlled crack.
Oxidized at 1375°C, 240 hr. and Polished	36	0.24-0.47	Failed due to SCG from a controlled crack.
Oxidized at 1375°C, 240 hr. and Polished	47	0.16-0.34	Failed due to SCG from a controlled crack.
Oxidized at 1450°C, 240 hr. and Polished	-	-	Broke at 117 MN/m^2 (17 ksi). No SCG.
Oxidized at 1450°C, 240 hr. and [illegible]ish	-	-	Broke at 172 MN/m^2 (25 ksi). No SCG.

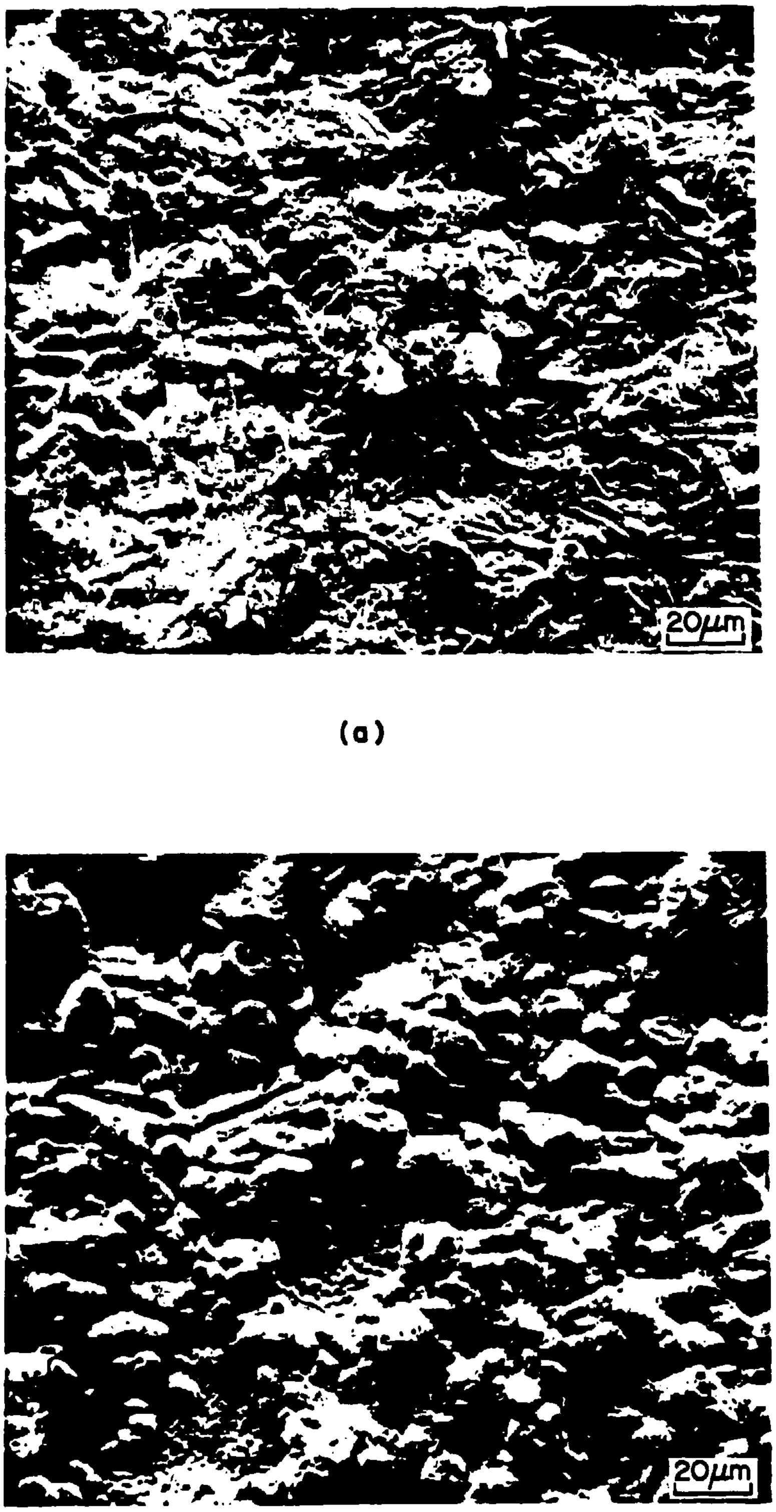

(a)

(b)

Figure 1.

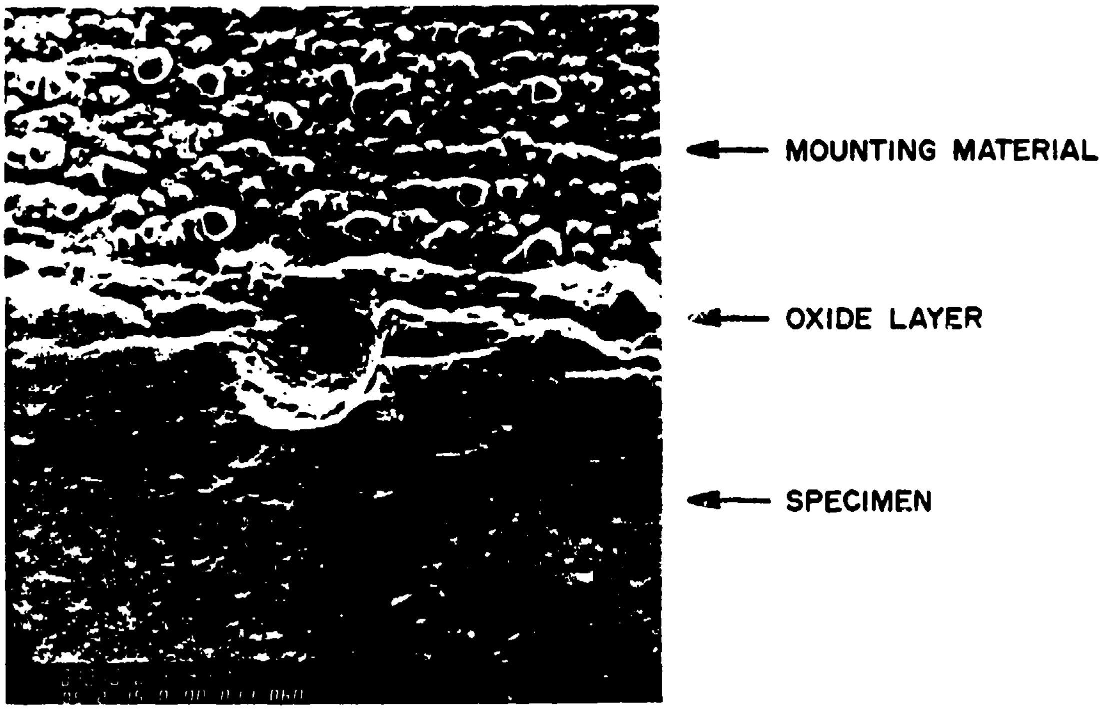

Figure 2.

Figure 3.

Figure 4.

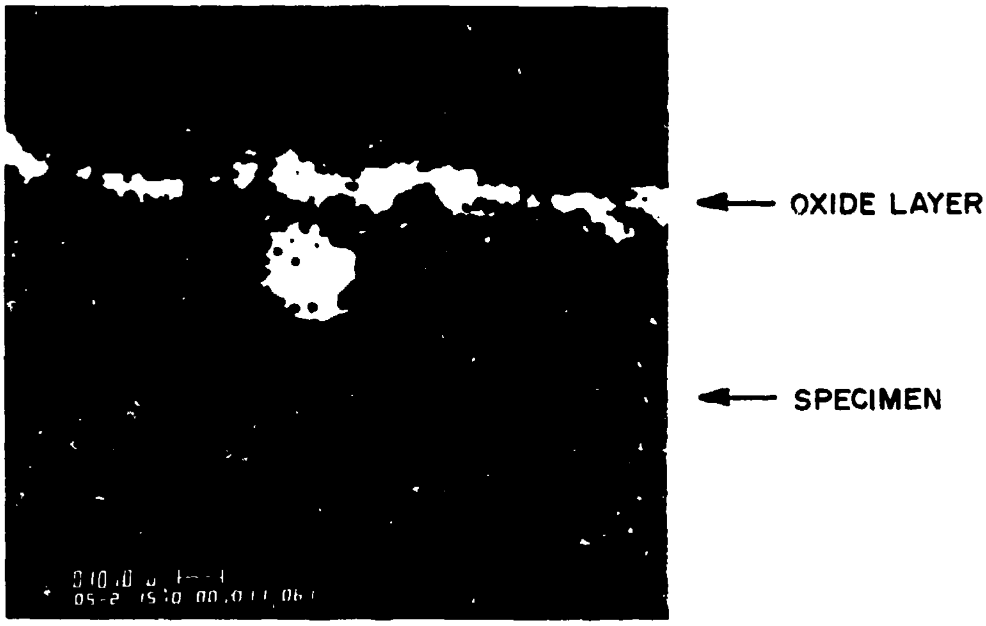

Figure 5.

AS-OXIDIZED LAYER
(a)

15µm REMOVED
(b)

22.5µm REMOVED
(c)

Figure 6.

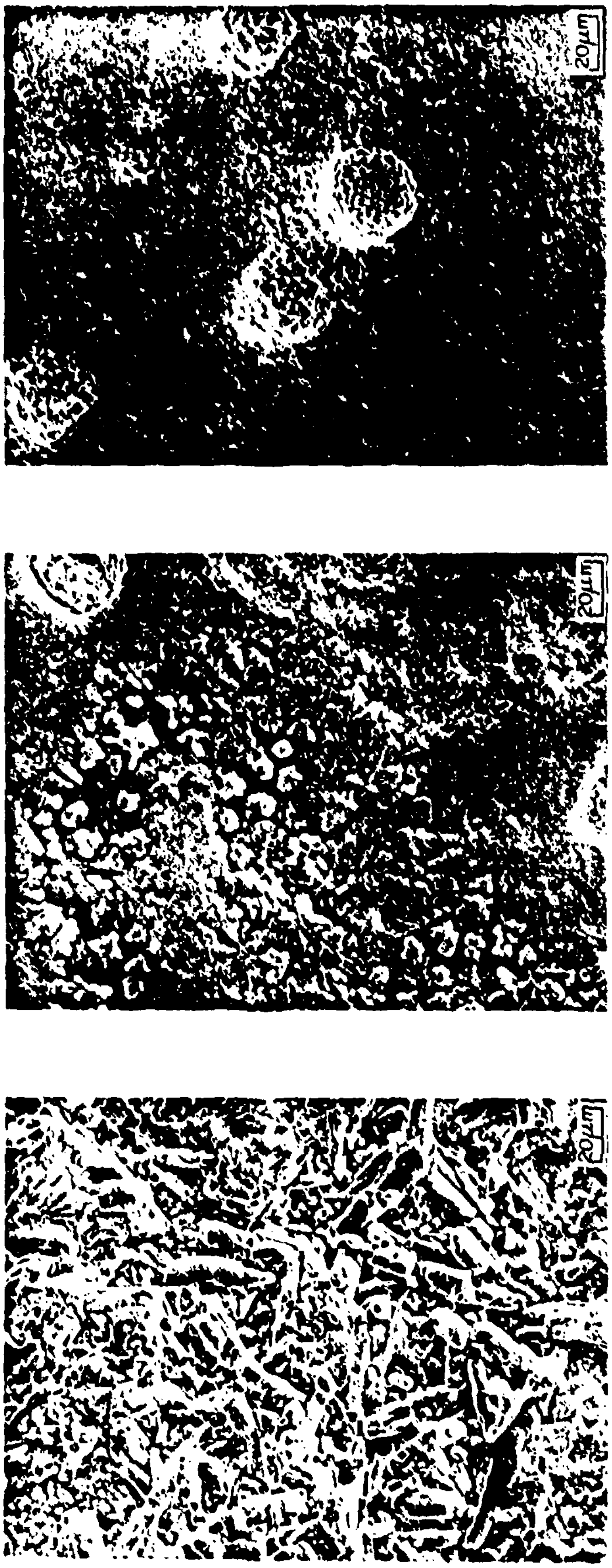

2.5μm REMOVED
(a)

25μm REMOVED
(b)

50μm REMOVED
(c)

Figure 7.

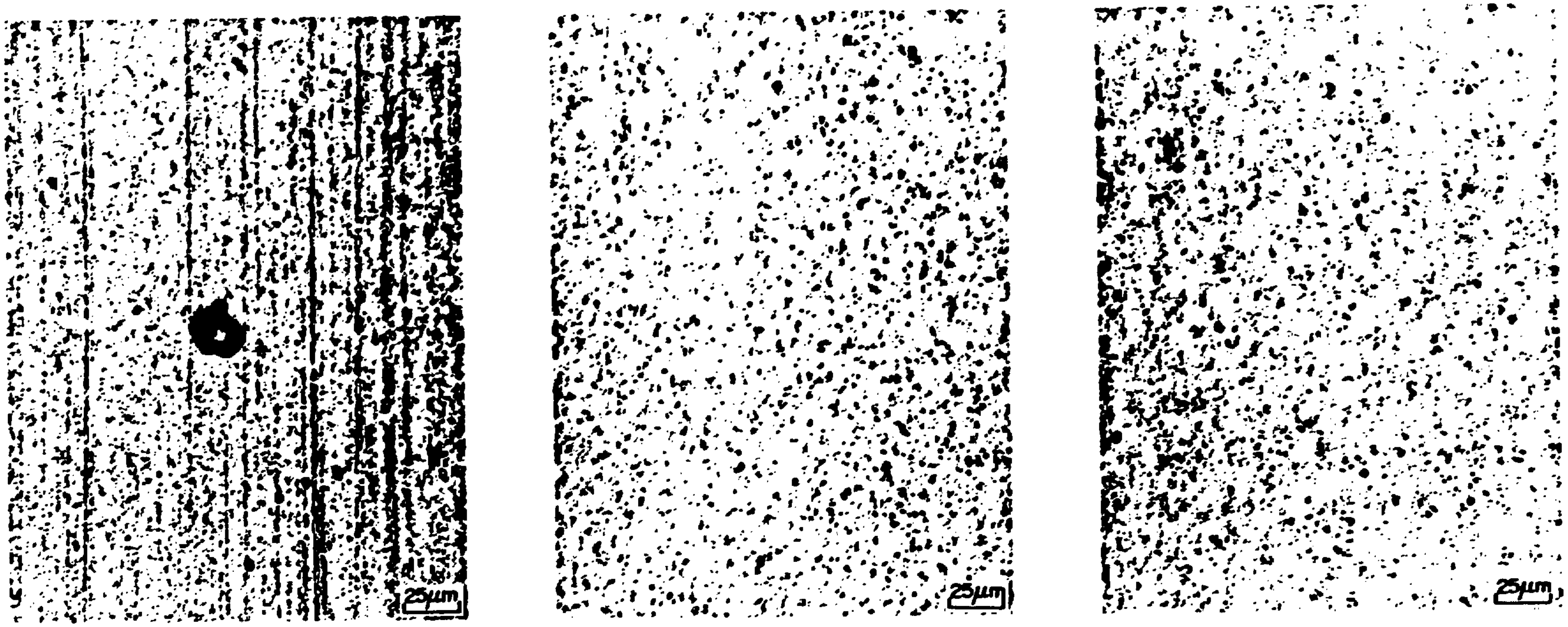

12µm REMOVED

(a)

25µm REMOVED

(b)

50µm REMOVED

(c)

Figure 8.

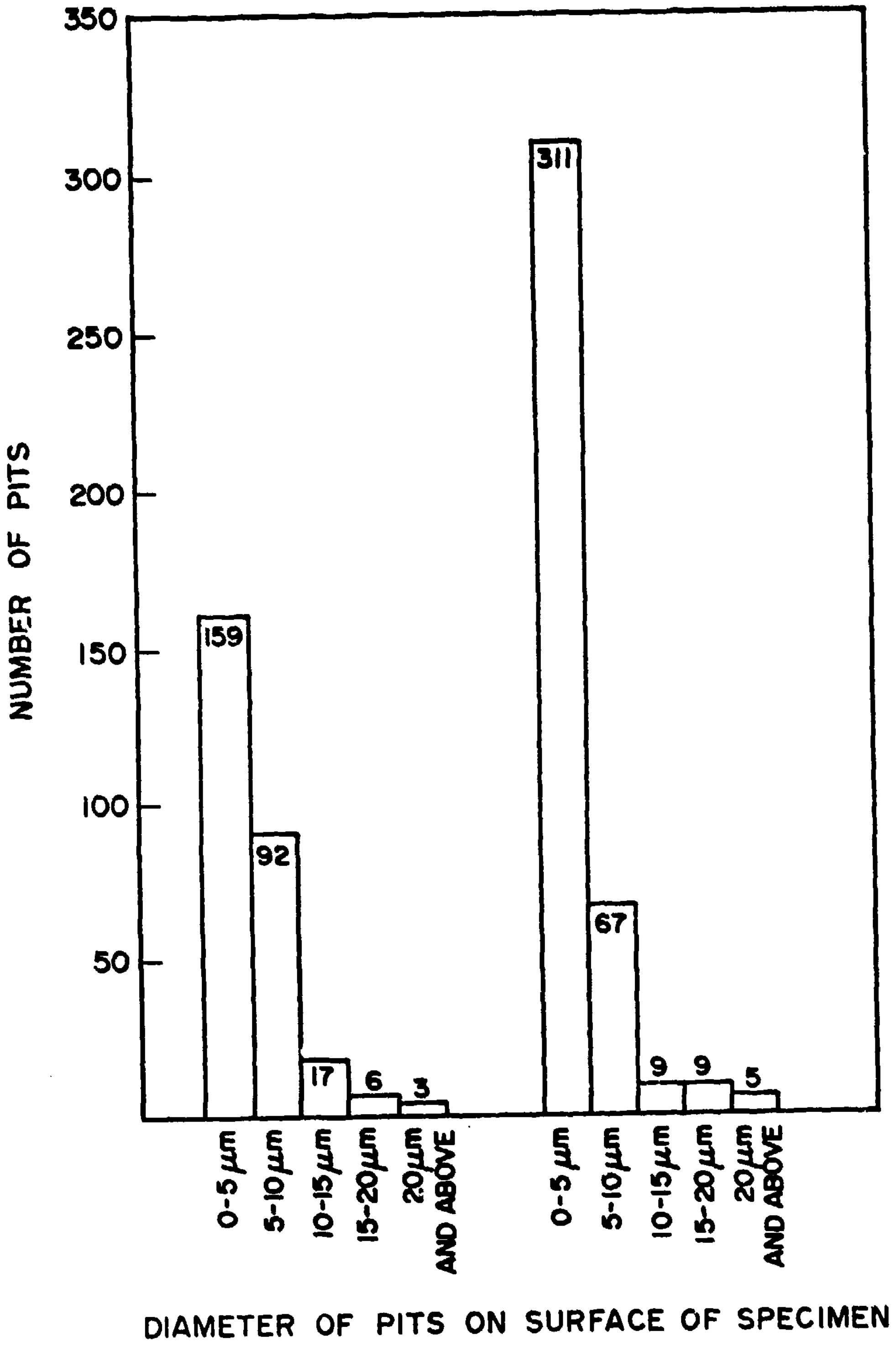
350
300
250
200
150
100
50
NUMBER OF PITS
159
92
17
6
3
311
67
9
9
5
0-5 μm
5-10 μm
10-15 μm
15-20 μm
20 μm AND ABOVE
0-5 μm
5-10 μm
10-15 μm
15-20 μm
20 μm AND ABOVE
DIAMETER OF PITS ON SURFACE OF SPECIMEN

Figure 9.

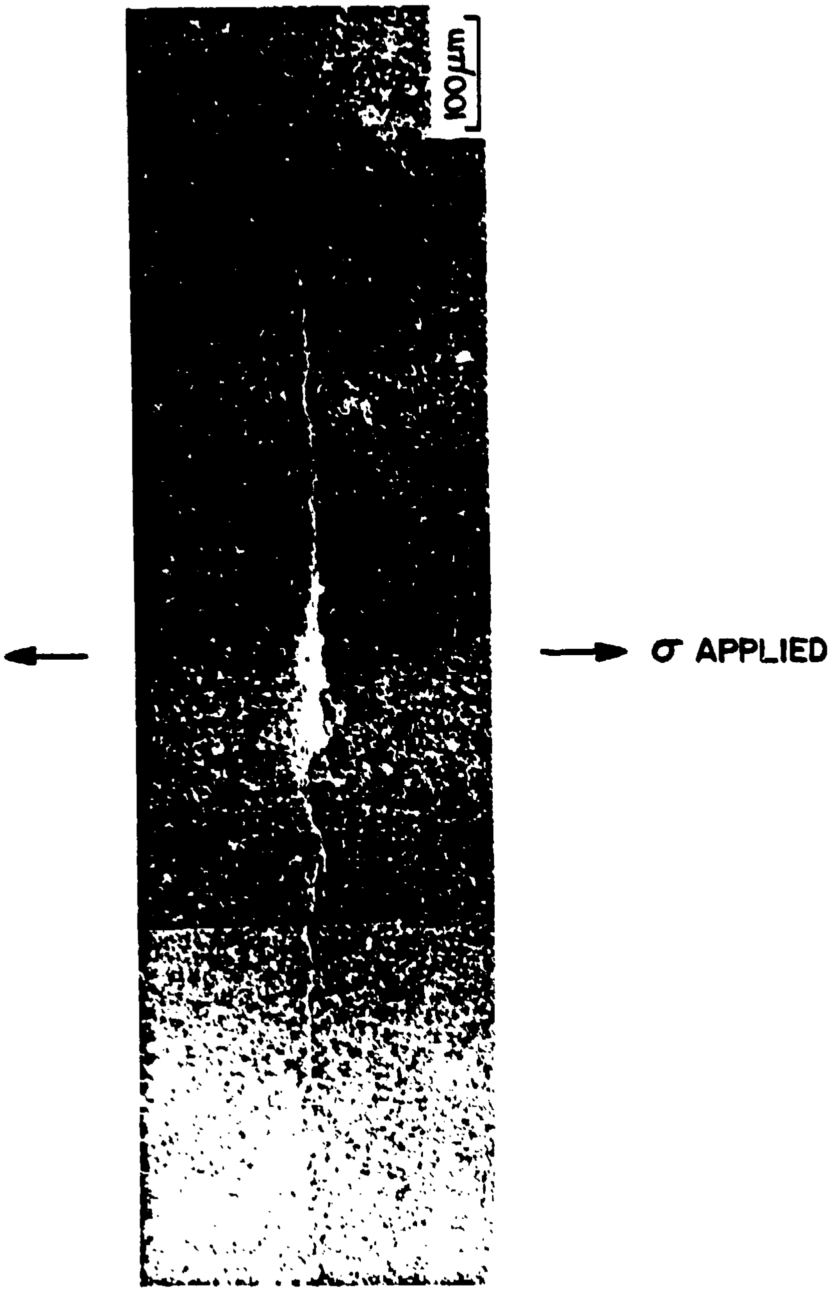

Figure 10.

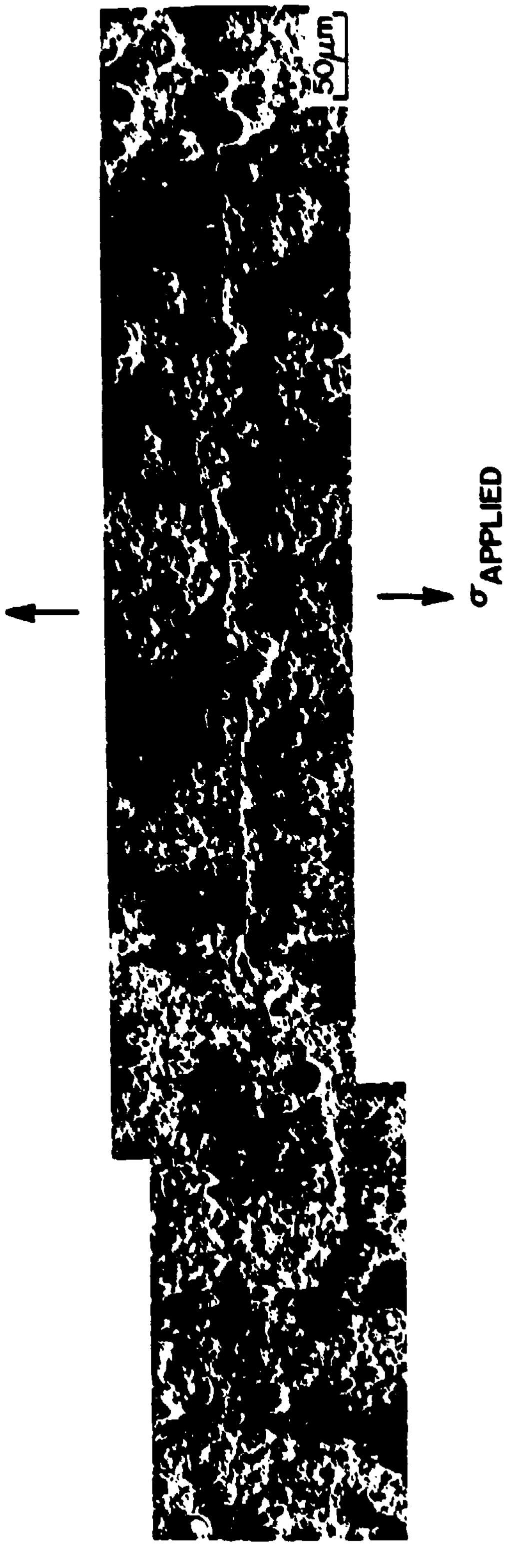

Figure 11.

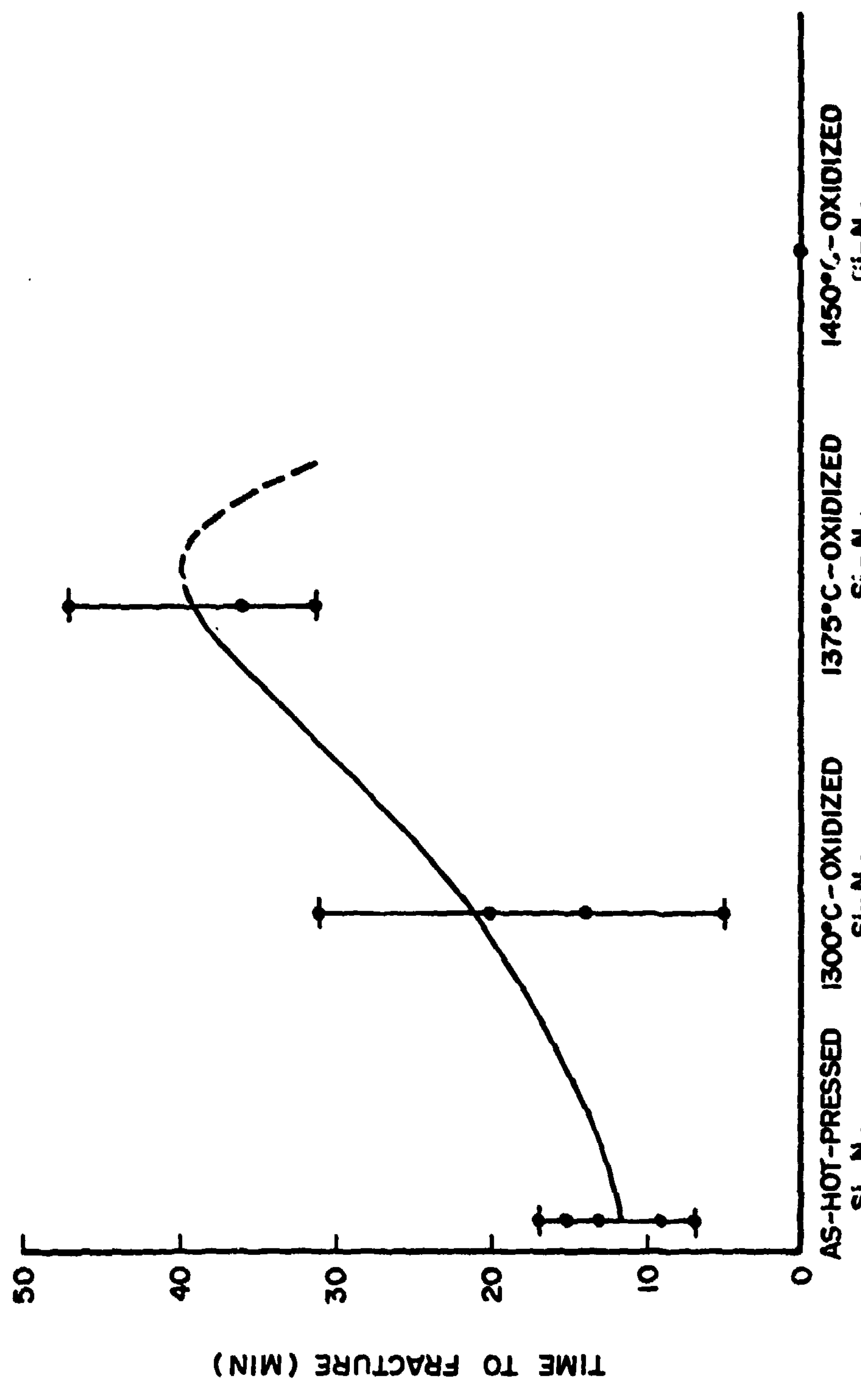
TIME TO FRACTURE (MIN)
0
10
20
30
40
50
AS-HOT-PRESSED Si_3N_4
1300°C-OXIDIZED Si_3N_4
1375°C-OXIDIZED Si_3N_4
1450°C-OXIDIZED Si_3N_4

Figure 12.

FLAW GROWTH IN A POLYCRYSTALLINE LITHIUM-ALUMINUM-SILICATE GLASS CERAMIC

B. S. Majumdar, T. Mah, and M. G. Mendiratta

Systems Research Laboratories, Inc.
2800 Indian Ripple Road
Dayton, Ohio 45440

ABSTRACT

The growth of indentation-produced "controlled" flaws in a polycrystalline lithium-aluminum-silicate glass ceramic has been studied, over a wide range of temperatures and strain rates. Significant scatter in the fracture stress at elevated temperatures suggests that the extent of slow crack growth is highly sensitive to microstructural details. The initial flaw shape is important in K_{IC} determination. Up to 1000°C the fracture toughness, K_{IC}, is essentially strain-rate insenstive, however, it decreases with temperature beyond 850°C. Intergranular cavity formation is suggested as the reason. Crack blunting by diffusive crack healing probably occurs at high temperatures. Also, intergranular slow crack growth occurs essentially under Mode I loading.

1. Introduction

Controlled-flaw growth experiments have recently been used to study the fracture behavior of structural ceramics. The controlled flaws are produced by indenting the specimen surface with diamond indentions. These flaws are typically 100 μm, to simulate the growth of naturally occurring flaws.

The overall fracture process involves the following: a) indentation cracking, b) slow crack growth (only at high temperature), and c) fast fracture. At present a few fairly good, although approximate, theoretical models on indentation crack have been developed, [1-4]. Yet, as will be shown in this paper, certain aspects of indentation cracking require further development. Slow crack growth at high temperatures in polycrystalline ceramics is generally intergranular in nature. As shown in Ref. 5, such intergranular fracture is not the corrosion-type phenomenon observed at room temperature in adverse environments. In time-to-failure and proof-stress calculations, it is generally assumed that the stress-intensity exponent n, in the equation $v = AK^n$, is a material constant which is independent of local chemical and microstructural heterogeneities. This assumption warrants critical analysis. Finally, the temperature dependence of the stress-intensity factor at unstable fracture requires further study.

The present study was conducted on a model material, polycrystalline Lithium-Aluminum-Silicate (LAS) glass ceramic, over a wide range of temperatures and loading rates. In addition, critical experiments were conducted in order to determine the effect of crack healing/blunting at high temperatures and also to investigate the effect of Mode II loading upon slow crack growth. All fracture tests were performed in four-point bending.

2. Experimental Procedure

The LAS glass ceramic, purchased from Corning (# 9617) was cut into bend bars approximately 50 mm long × 8 mm wide × 4 mm thick. The approximate composition (%) of the material was

Li	Al	Mg	Ti	Zn	Zr	Fe	Ca	Na	Si
1.6	11.3	1.4	2.4	1.5	0.1	0.2	0.1	0.2	major

The bars were ground on emery paper in order to remove any coating remaining from prior finishing treatments. The tension side of each band bar was then carefully mechanically polished (up to 15μ finish) using diamond paste. The cleaned samples were then annealed in air at 1100°C for 3 h. The bars were subjected to the annealing treatment in order to homogenize the microstructure. Experience with unannealed samples showed low strength and significant scatter in the fracture stress; the annealing treatment reduced the scatter considerably. After annealing,single indents were made at the center of the tension side of the specimens, using a Vicker's diamond pyramid indentor. The indentor was oriented such that one set of radial cracks was aligned perpendicular to the maximum normal-stress direction. As a result these radial cracks behaved as Mode I flaws for subsequent fracture testing. Fig. 1 is a sketch of the geometry of the fracture samples. The indentor load was 2500 gm., producing radial cracks ~ 110 μm in length. Fracture tests were also performed with Knoop indents, but the cracks produced were not always sharp and sufficiently deep and, as a result, final fracture did not always originate from the indents.

In some tests the indentor was oriented in such a way as to produce radial cracks at various angles to the principal normal-stress direction. These tests were carried out in order to evalute crack propagation under a combination of Modes I, II, and III loading conditions and to determine whether intergranular slow crack growth occurs under mixed-mode loading.

Fracture testing was conducted in the Instron at temperatures ranging from room temperature to 1100°C, in air and in vacuum (10^{-4} Torr) environments. Testing was initiated 20 min. after the desired temperature was reached. Cross-head speeds ranged from 0.005 to 1.25 cm/min., resulting in strain rates between $\simeq 3 \times 10^{-5}$/sec. and $\simeq 7 \times 10^{-3}$/sec. or the tension surface.

The loading rate was varied in order to obtain different extents of slow crack growth. After fracture the fracture surfaces were coated with gold and observed in a Cambridge scanning electron microscope. The indented crack region and the zone of slow crack growth were easily discernible; therefore, K_{IC} could be determined from the crack size and load at fracture. Special features on the fracture surfaces were also noted.

3. Results and discussion

3.1 Fracture stress

Fig. 2 shows the variation of fracture stress with cross-head speed at 1000°C. For all samples the indented radial cracks were oriented normal to the maximum principal stress direction. The data points correspond to tests conducted in 10^{-4} -Torr vacuum. Results of tests conducted in air show no significant deviation from the vacuum data. Table I summarizes the test results. Fig. 3 is a schematic of the fracture surface, showing regions of indented crack, slow crack growth, and fast fracture. The indented crack is nearly semicircular in shape. However, following slow crack growth, there is a change in shape of the crack front. The ratio a/c quantifies the ellipticity of the flaw at fast fracture. Table I shows a wide variation of a/c ratios. Nevertheless, there is always a general tendency for slow crack growth to occur along the length direction rather than along the depth, yielding a/c ratios less than unity.

Two other features in Fig. 2 are notable. The first is the significant scatter in the fracture stress, although fast fracture always originated at the indent. Similar scatter was observed in hot-pressed silicon nitride [6].

It is believed that such scatter is mainly caused by the irregular behavior of slow crack growth, which results in variations of the flaw size and shape prior to fast fracture. However, in spite of the scatter, the fracture stress seems to increase monotonically with the strain rate. This behavior may be contrasted with the results obtained in Ref. 7, where it was found that beyond a certain strain rate, the fracture stress decreased with an increase in strain rate. When the data in Fig. 2 are plotted on a log-log scale, in a manner normally employed in dynamic fatigue experiments, a stress-intensity exponent of ~ 6.5 is obtained. Here the stress-intensity exponent corresponds to n in the equation $\sigma_f = A\, \dot{\sigma}^{\,1/n+1}$ or $v = B\, K^n$, where $\dot{\sigma}$ is the stress rate, v the crack velocity, K the stress-intensity factor, σ_f the fracture stress, and A and B are constants. The value of n is quite reasonable. For example, in silicon nitride, n ranges from 8 to 12 [8,9]. The other notable feature in Fig. 2 is the significant decrease in fracture stress from room temperature (135 MPa) to 1000°C (42 MPa) at a cross-head speed of 0.005 cm/min. Further comments on this decrease will be made in a later section of this paper.

3.2 Fracture toughness

The fracture toughness, K_{IC}, can be calculated from the fracture stress, flaw size, and flaw shape at fast fracture. The critical flaw is taken to be the outer boundary of the slow-crack-growth regime. This boundary can always be delineated from the SEM micrographs. Fig. 4 is a micrograph of a fracture surface, showing well-defined regions A, B, and C which correspond to domains of the indented crack, slow crack growth, and fast fracture, respectively. Not always is the extent of slow crack growth so uniform in all directions as it is in Fig. 4. In any case, the final flaw shape was always approximated by a semi-ellipse, with the length of the flaw on the surface being set equal to '2c', and the depth being set equal to 'a' (see Fig. 3).

The value of K_{IC} was obtained at a point corresponding to the location of the maximum stress-intensity factor, along the flaw boundary. The appropriate formula for K_{IC}, obtained from Ref. 10, was

$$K_{IC} = \frac{2\sigma_f\sqrt{a}}{Z} \qquad (1)$$

where σ_f is the fracture stress, 'a' the flaw depth, and Z a crack shape parameter, viz.,

$$Z = E(k) \qquad \text{for } a \leq c$$
$$= \sqrt{\frac{a}{c}}\ E(k') \qquad \text{for } a \geq c$$

E(k) and E(k') are the complete elliptic integrals of the second kind, with modulus $k = \sqrt{1 - a^2/c^2}$ and $k' = \sqrt{1 - c^2/a^2}$, respectively. Note that for $a/c \leq 1$, the maximum stress intensity occurs at the depth, and for $a/c \geq 1$ it occurs at the surface.

Using the formulae given above, K_{IC} was determined for various specimens. Fig. 5 shows the variation of K_{IC} with strain rate at 1000°C. Within the range of data available, K_{IC} is essentially a constant, equal to 0.5 $\text{MPa}\sqrt{\text{m}}$. Of particular importance is the sharp decrease in scatter of the data, as compared to that in Fig. 2. For example, at a cross-head speed of 0.005 cm/min., the scatter in fracture stress is ± 25%, while the scatter in K_{IC} is only ± 5%.

Such behavior is expected if fracture toughness controls the strength of a member. The large variation in fracture stress is thus explained as being due to the scatter in the extent of slow crack growth. This variability in the domain of slow crack growth remains to be explained, although local variations in the microstructure and chemistry may be responsible in part.

3.3 Temperature dependence of K_{IC}

Fig. 6 shows the temperature dependence of K_{IC}, at cross-head speeds of 0.005 and 0.05 cm/min. Data for tests conducted in both vacuum and air are included. Up to 850°C, K_{IC} remains essentially constant at 1.4 MPa$\sqrt{m}$. Beyond that temperature K_{IC} decreases with temperature, reaching ~ 0.5 Mpa$\sqrt{m}$ at 1000°C. The behavior is opposite that observed in hot-pressed silicon nitride [7], where the fracture toughness was found to increase with temperature. However, K_{IC} dependence, similar to that presently observed, has been reported in hot-pressed silicon carbide [11].

At still higher temperatures the value of K at instability depends quite sensitively upon strain rate. Thus, in vacuum at 1100°C, K_{IC} increases from 0.26 to 0.79 MPa$\sqrt{m}$, for an increase in cross-head speed of 0.005 to 0.05 cm/min. In air the increase is from 0.26 to 0.6 MPa$\sqrt{m}$, for the same range of cross-head speeds. It will be shown later that a significant fraction of intergranular damage occurs in the fast-fracture region at 1100°C. Such intergranular damage probably explains the strain-rate dependence of the fracture stress, since intergranular fracture is generally rate sensitive.

The curve in Fig. 6 which corresponds to a cross-head speed of 0.005 cm/min. shows that the effective surface energy γ ($\gamma = \frac{K^2}{4E}$) is ~ 450 ergs/cm^2 at 1100°C. The surface energy of the grain-boundary liquid phase of the material under investigation is not known. However, a rough comparison may be made with liquid sodium silicate, whose surface energy is 250 ergs/cm^2 at 1000°C [12]. Extrapolation of the curve in Fig. 6 shows that the surface energy of the present material would be 250 ergs/cm^2 at 1170°C. Bearing in mind that the eutectic temperature of β-spodumiene lies between 900 and 1000°C, and provided that crystalites do not become glassy, a temperature of 1200°C should be sufficient for complete intergranular fracture to occur at a cross-head speed of 0.005 cm/min.

The decrease of K_{IC} with temperature needs some explanation. One possibility is the modulus effect, arrived at through the equation $K_{IC} = 2\sqrt{E\gamma}$. It is known that E is a very insensitive function of temperature. Therefore, the nearly three-fold decrease in K_{IC} from 850 to 1000°C cannot be explained by changes in E. Clearly this is unlikely. The second possibility is based upon the premise that γ decreases with temperature. Note that γ is actually the free-energy increase of the solid-per-unit increase in surface area, at constant volume and temperature [13]. Thus,

$$\gamma = U_s - TS_s \tag{2}$$

where U_s and S_s are, respectively, the energy and entropy change associated with formation of the surface. Under the assumption that U_s and S_s are temperature independent,* one obtains

$$\gamma|_{T_2} - \gamma|_{T_1} = (T_1 - T_2)S_s \tag{3}$$

---

*Valid for several solid-liquid, solid-vapor interfaces of metals [13].

The value of S_s is not known for the present material. However, for several metals it ranges from 0.5 to 3 ergs/cm^2 °K [13]. Using the latter value for S_s,

$$\gamma|_{1000^\circ C} - \gamma|_{850^\circ C} = 450 \text{ ergs/cm}^2. \tag{4}$$

Using the data for K_{IC} and a modulus of 7.6 × 10^4 MPa, for the present material, one obtains

$$\gamma|_{1000^\circ C} - \gamma|_{850^\circ C} = 11{,}200 \text{ ergs/cm}^2. \tag{5}$$

This value is an order of magnitude higher than that predicted by Equation 4. Thus, the entropy effect is also unable to explain the temperature dependence of K_{IC}. It will be shown later that intergranular damage and cavity formation in the fast-fracture region offer an explanation for the temperature dependence of K_{IC}.

3.4 Fractography

Fig. 7 is a micrograph of the fracture surface of a sample tested at room temperature. Figs. 8 and 9 are higher-magnification micrographs in the indented-crack region and fast-fracture region, respectively. In both zones fracture is of the cleavage type. However, the distinct difference in morphology is worth noting. The fracture is directional and smooth in Fig. 8 and rough in Fig. 9. It is possible that the change in morphology occurs because of a difference in crack-growth rate in the two regimes. However, it is difficult to reconcile this possibility with the fact that a discontinuous change occurs in the fracture-surface morphology at the boundary between the indented-crack zone and the fast-fracture zone. If the morphology is simply velocity related, a transition zone should be observed in which the morphology changes gradually. The indentation process generates complex stress states involving an elasto-plastic deformation field. Therefore, the morphological differences may be associated with different stress states existing during indentation and fast fracture.

At temperatures of 1000°C and above, a distinct zone of slow crack growth is observed (Fig. 3). Fracture is intergranular in the slow-crack-growth region, as shown in Fig. 10. At these high temperatures, a significant fraction of the grain boundaries is occupied by a liquid glassy phase. Since this phase would normally have lower surface energy than the interior of the grains, fracture should occur primarily along the grain boundaries. Such grain-boundary failure is thermally activated; therefore, the extent of slow crack growth would be cross-head-speed dependent which, in turn, would be manifested as an increase in fracture stress with strain rate, as shown in Fig. 2.

Closer observation of Fig. 10 shows a number of river lines, suggesting that transgranular cleavage fracture is present in addition to separation along the grain-boundary liquid phase. However, brittle failure along the remaining solid grain-boundary amorphous phase cannot be ruled out. Fig. 11 is a higher-magnification micrograph of Fig. 10, showing relative rotation and separation along the grain boundaries. The process of intergranular fracture may, therefore, be summed up as follows: a) formulation of a liquid glassy phase along grain boundaries, b) relative sliding and rotation between grains, giving rise to cavities, and c) final separation between grains.

It must be noted, however, that such intergranular fracture involves competition with a crack-healing process, especially because of the presence of the liquid glassy phase. In fact, there is indirect evidence that such a crack-healing process took place in the present material. This will be discussed in a later section of this paper.

Fig. 12 is a high-magnification micrograph showing regions immediately below the indentor (A), the indented crack (B), and the slow-crack-growth regime (C). The intergranular-type fracture immediately below the indentor should be noted. This feature was characteristic of most samples tested at high temperature. Such intergranular fracture is consistent with theories [3,4] stating that during indentation, crack initiation occurs at a finite depth below the indentor, and not at the surface. The region immediately beneath the indentor may remain uncracked (or partially cracked); thus, the indented crack is really annular shaped rather than semicircular.

Fig. 13 is an SEM micrograph in the fast-fracture region of a sample tested at 1000°C. Fracture is essentially of the cleavage type, although many of the cleavage steps are obscured by the glassy phase formed at the high temperature. In addition, a large number of cavities may be seen, having formed mainly at the triple points of the grain boundaries. It is very likely that the triple points have a higher concentration of the glassy phase. The nature of the microcracks suggests grain-boundary sliding and rotation. Sliding is a distinct possibility since at the high temperatures, the grain boundaries form liquid phases having fairly low surface energies ($\simeq 250$ ergs/cm^2). It is believed that nucleation of grain-boundary microcracks occurs in the stress field ahead of the main crack. Since plasticity within the grains is negligible even at high temperatures, the stress field can only be relaxed by relative sliding of the grain boundaries. Weaker bonding at the grain boundaries allows such phenemena. It is interesting to note that microcracks were not observed near the side surfaces of the samples. This observation suggests that a plane-strain tensile hydrostatic field is necessary for formation of cavities. This is consistent with the fact that for relative sliding of two surfaces to occur, a combination of shear and tensile stresses makes sliding easier as compared to the case where only shear stress is present. Also a tensile field would naturally aid the opening up of microcracks.

The formation of microcracks ahead of the main crack has important implications. Their presence would locally increase the stress-intensity factor of the main crack. Essentially this is a "crack-aiding" phenemenon, as opposed to the "shielding" of cracks when dislocations are emitted from crack tips [14]. The aiding of crack propagation by microcracks formed ahead of a main crack has also been mentioned by Evans and Wiederhorn [8] in their work on silicon nitride. Some calculations are given in Ref. 15. The calculations are rough and, therefore, no quantitative effect of microcracks has been assessed in this work. Nevertheless, the presence of microcracks in the fast-fracture region probably explains the sharp decrease in K_{IC} with temperatures of 850°C and above.

At 850°C cavities are absent in the fast-fracture region. The fracture surface is similar to that observed at room temperature. Fig. 14 shows the fast-fracture region of a sample tested at 1100°C at 0.005 cm/min. The significant size and number of cavities is noteworthy. This micrograph should be compared with Fig. 13. Thus, as testing temperature is increased beyond 850°C, cavities begin to appear and their size increases gradually. These observations may be compounded with the K_{IC} data at 0.005 cm/min. (Fig. 4), which shows the fracture toughness to decrease from 1.4 to 0.26 $MPa\sqrt{m}$ in the temperature range 850 - 1100°C. Fractographic analysis of a specimen tested in air at 1100°C at 0.2 cm/min. showed fewer and smaller cavities, compared to those in Fig. 14. Here, also, the observation is consistent with the fact that K_{IC} was 0.4 $MPa\sqrt{m}$ at 0.2 cm/min., compared to 0.26 $MPa\sqrt{m}$ at 0.005 cm/min.

Figure 15 shows the fast-fracture region in a specimen tested at 925°C. In this case the cavities were unevenly distributed, with certain regions showing intergranular cavities and others showing no cavities at all. The intergranular damage is thus intermediate between 850 and 1000°C. A K_{IC} of 0.8 $MPa\sqrt{m}$ at 925°C is, therefore, understandable. These micrographs suggest that a "mixture" theory of transgranular and intergranular damage might explain the observed K_{IC} dependence upon temperature. It should also be mentioned that a gradual transition takes place in the fracture-surface topography from 850 to 1100°C, the fast-fracture regions becoming progressively smoother or flatter. The behavior of K_{IC} may also depend upon such transition in topography. However, cavities probably play a more dominant role in lowering K_{IC}.

3.5 Crack-blunting phenemenon

As previously mentioned, crack blunting by the viscous grain-boundary phase is a distinct possibility. To test this hypothesis, a specimen was indented at room temperature and then annealed in air at 1100°C for 3 h. Subsequent fracture testing at room temperature yielded a K_{IC} of 2 MPa$\sqrt{m}$ for specimens tested at room temperature immediately following indentation. As expected, the fast-fracture region was similar for the two types of specimens. The increase in K_{IC} for the annealed sample can, therefore, be explained only by some extent of crack healing and rounding of the crack tip by flow of the viscous glassy phase. A healing phenemenon was also inferred from the observation that in the annealed sample, voids were present in the boundary region between the indented and fast-fracture domains (Fig. 16). These voids presumably were left behind during the healing process, as suggested by Evans and Charles [15]. The viscous glassy phase should be rich in lithium; therefore, the boundary region should show a larger concentration of this element, as compared to the remainder of the fracture surface. Unavailability of Auger equipment prevented further work in this area.

3.5 Inclined cracks

Limited tests were conducted at 1000°C with indented cracks inclined at an angle to the maximum principal stress direction. The purpose was to determine the crack path and also whether slow crack growth was occurring under Mode II conditions. Indented cracks were made at angles of 30 and 45 deg. (Fig. 17).

The dashed line in Fig. 17 shows schematically the general fracture path. Fracture tended to become normal to the bending-stress direction in all cases. In fact, when θ was 45 deg., fast fracture took place along the square edge of the indent. Presumably the median cracks terminate along the square edges of the indentor.

Figs. 18(a) and (b) show two views of the crack path when $\theta = 30$ deg. In Fig. 18(a) the specimen has been tilted with respect to the electron beam, in such a way that both the side surface (bottom dark region) and fracture surface (top bright region) are visible. Fast fracture originated from the inclined indent; however, note (on the left side of the micrograph) that the crack gradually becomes orthogonal to the principal normal stress direction. Fig. 18(b) shows that fast fracture did not completely follow the indent. Here too is an indication that indented cracks are annular rather than semicircular.

The top right-hand side of Fig. 18(a) shows intergranular slow crack growth which occurs perpendicular to the principal bending-stress direction. Intergranular fracture did not occur on crack surfaces inclined at an angle to the bending-stress direction. These observations lead to the conclusion that slow crack growth occurs primarily under Mode I loading conditions.

4. Conclusions

i) Fracture always occurs at the indent, indicating that the indentation crack may be used as a standard precrack for ceramics.

ii) At room temperature the indented fracture surface differs from the fast-fracture surface, and the morphology changes discontinuously in the boundary region. Mixed-mode cracking during indentation is suggested as a possible reason.

iii) Intergranular fracture (at high temperatures) in the region just below the indent verifies that cracking may not occur there during indentation.

iv) Large scatter in the fracture stress indicates that the extent of slow crack growth (also verified fractographically) is highly sensitive to microstructural and local chemical heterogenities; this has important implications in proof-stress design.

v) The initial flaw shape is important in K_{IC} determination.

vi) Over a wide temperature range, K_{IC} is independent of strain rate.

vii) K_{IC} decreases significantly with temperature beyond 850°C. Intergranular cavity formation is cited as the reason.

viii) Crack healing and blunting do occur at high temperatures.

ix) Intergranular slow crack growth occurs essentially under Mode I conditions, even when other modes are present.

Acknowledgement

The authors would like to thank Messrs. Mark Rowe and George Cornish for conducting the mechanical testing. This work was supported under Contract F49620-77-C-0124 with the Air Force Office of Scientific Research.

References

1. D. B. Marshall and B. R. Lawn, J. Mater. Sci. 14 (1979) 2001.
2. D. B. Marshall, B. R. Lawn, and P. Chantikul, J. Mater. Sci. 14 (1979) 2225.

3. B. R. Lawn and A. G. Evans, J. Mater. Sci. 12 (1977) 2195.

4. B. R. Lawn and M. V. Swain, J. Mater. Sci. 10 (1975) 113.

5. F. F. Lange, J. Amer. Ceram. Soc., 57 (1974) 84.

6. M. G. Mendiratta and J. J. Petrovic, J. Amer. Ceram. Soc. 61 (1978) 226.

7. R. K. Govila, K. R. Kinsman, and P. Beardmore, J. Mater. Sci. 13 (1978) 2081.

8. A. G. Evans and S. M. Wiederhorn, J. Mater. Sci. 9 (1974) 270.

9. F. F. Lange and J. L. Iskoe, Proceedings of the Second Army Materials Technology Conference (held at Hyannis, MA, November 13-16, 1973) (Eds., J. J. Burke, A. E. Gorum, and R. N. Katz) (Brook Hill Publishing Co., 1974).

10. G. K. Bansal, J. Amer. Ceram. Soc. 59 (1976) 87.

11. J. J. Petrovic and L. A. Jacobson, J. Amer. Ceram. Soc. 59 (1976) 34.

12. W. D. Kingery, Introduction to Ceramics, (John Wiley and Sons, Inc., N.Y., 1963).

13. R. A. Swalin, Thermodynamics of Solids (John Wiley and Sons, Inc. N.Y., 1972).

14. B. S. Majumdar and S. J. Burns, Acta Met. 29 (1981) 579.

15. A. G. Evans and E. A. Charles, Acta Met. 25 (1977) 919.

LIST OF ILLUSTRATIONS

Figure 1. Schematic of Indented Specimen and Loading Arrangement.

Figure 2. Variation of Fracture Stress with Cross-Head Speed at 1000°C in Vacuum.

Figure 3. Schematic Showing Regions of Indented Crack, Slow Crack Growth, and Fast Fracture. The flaw shape at fast fracture is approximated by a semi-ellipse of length "2c" and depth "a".

Figure 4. SEM of the Fracture Surface of a Sample Tested at 1000°C and 0.005 cm/min; A - Indented Crack, B - Slow Crack Growth, C - Fast Fracture.

Figure 5. Variation of K_{IC} with Cross-Head Speed at 1000°C.

Figure 6. Variation of K_{IC} with Temperature For Specimens Tested in Vacuum; ⊙ - 0.005 cm/min., △ - 0.05 cm/min. Cross-Head Speed.

Figure 7. SEM of Fracture Surface of a Sample Tested at Room Temperature; A - Indented Crack, B - Fast Fracture. Note the discontinuous transition in fracture morphology at the boundary of Regions A and B.

Figure 8. Higher-Magnification Micrograph of Indented Crack Region of Fig. 7. Note the flat mirror-like feature.

Figure 9. Higher-Magnification Micrograph of Fast-Fracture Region of Fig. 7. Note the characteristic transgranular cleavage fracture.

Figure 10. SEM of the Slow-Crack-Growth Region of a Specimen Tested at 1000°C at 0.005 cm/min. Fracture is intergranular.

Figure 11. Higher-Magnification Micrograph of the Slow-Crack-Growth Region of a Specimen Tested at 1000°C.

LIST OF ILLUSTRATIONS (Cont'd)

Figure 12. SEM of Fracture Surface of a Specimen Tested at 1100°C, Showing Regions Immediately Below the Indentor (A), Indented Crack (B) and Slow-Crack Growth Regime (C). The intergranular fracture immediately below the indentor should be noted.

Figure 13. SEM of the Fast-Fracture Region of a Specimen Tested at 1000°C.

Figure 14. SEM of the Fast-Fracture Region of a Specimen Tested at 1100°C. The size and number of cavities in this micrograph may be compared with those in Fig. 13.

Figure 15. SEM of Fast-Fracture Region of a Specimen Tested at 925°C. Note that the cavities are unevenly distributed.

Figure 16. SEM of the Fracture Surface of a Specimen Near the Boundary of the Indented Crack (A) and the Fast Fracture (B). Specimen was fractured at room temperature following annealing of the indent at 1000°C. The voids in the boundary region should be noted.

Figure 17. Schematic Showing Fracture Path for Specimens with Angular Indent.

Figure 18. Two Views of the Fracture Surface of a Specimen with Angular Indent Fractured at 1000°C. The specimen has been tilted in the microscope so that both the side surface (bottom of [a] and bottom right of [b]) and fracture surface (top of [a] and top left of [b]) are visible.

TABLE I

T^oC	Rate cm/min	Fracture Stress σ_f, MPa	a/c	K_{IC} Mpa$\sqrt{m}$	Environment	Comments
25	0.005	135	1.057	1.73	air	
25	0.005	180	0.9	2.05	air	Indent was annealed in air at 1000°C for 3 h prior to fracture test.
850	0.005	120	0.73	1.5	vacuum	
925	0.005	81	1.07	0.8	vacuum	
1000	0.005	52	0.78	0.52	vacuum	
1000	0.05	51	1.18	0.48	vacuum	
1000	0.05	62	1.12	0.62	air	
1000	0.25	64	0.97	0.63	vacuum	
1050	0.005	35	0.67	0.38	air	
1100	0.005	28	0.93	0.29	vacuum	
1100	0.005	24	0.71	0.24	air	
1100	0.05	41	0.40	0.76	vacuum	
1100	0.05	33	0.26	0.58	air	
1100	0.20	49	0.78	0.44	air	
1100	0.30	56	1.11	0.55	air	
1000	0.005	60			vacuum	Angular indent
1000	0.005	58			Air	Angular indent

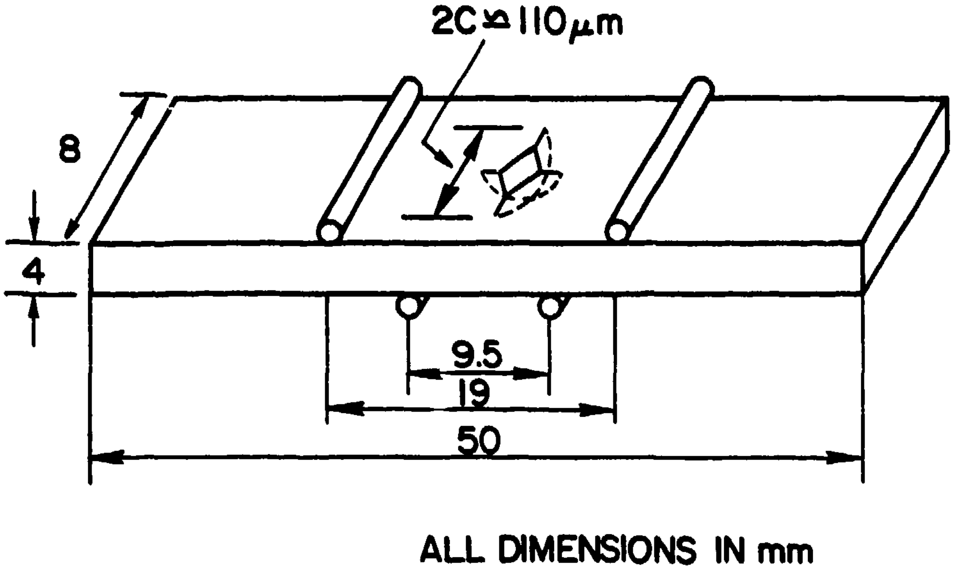

Figure 1.

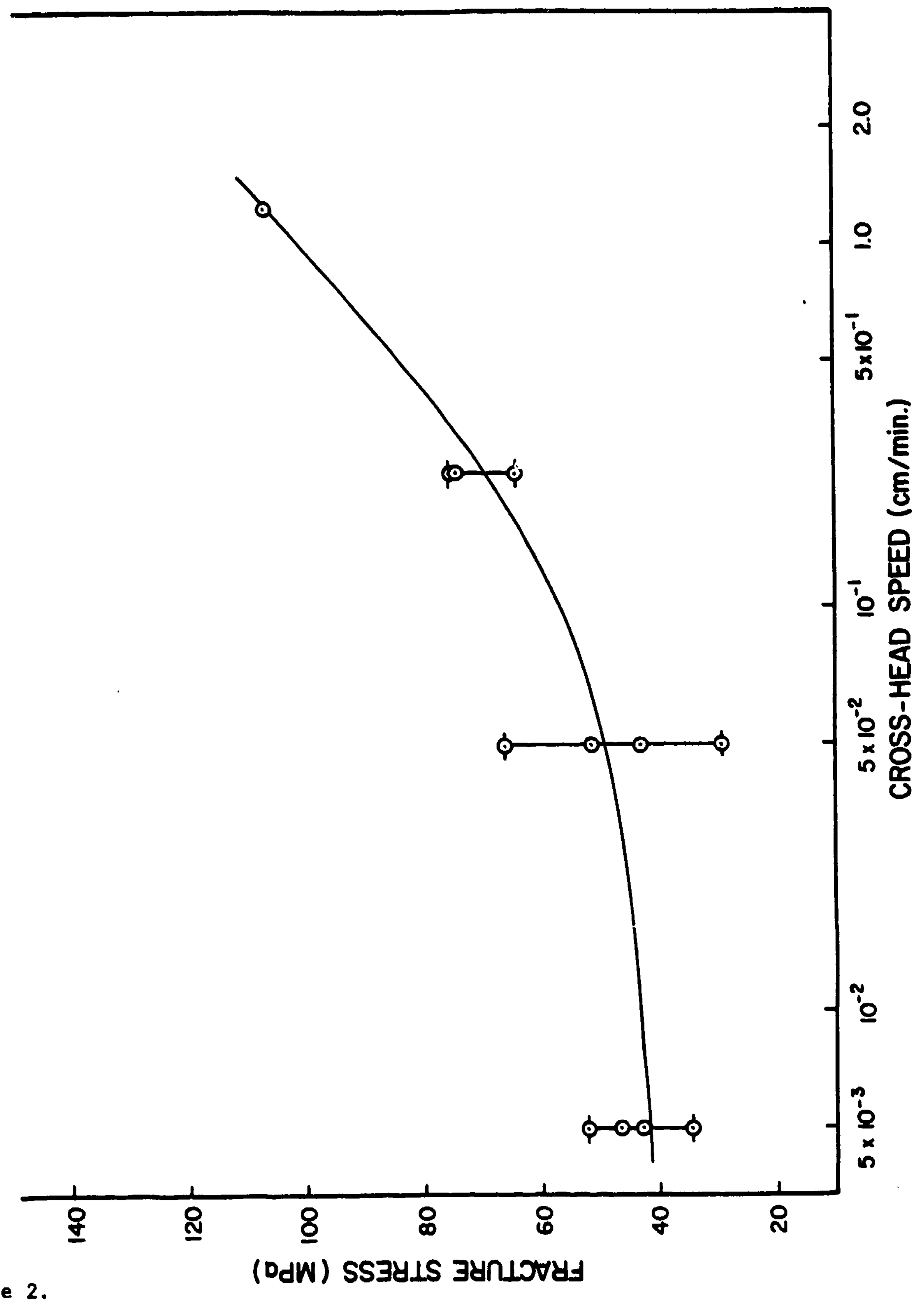
FRACTURE STRESS (MPa)
20
40
60
80
100
120
140
CROSS-HEAD SPEED (cm/min.)
5×10^{-3}
10^{-2}
5×10^{-2}
10^{-1}
5×10^{-1}
1.0
2.0

Figure 2.

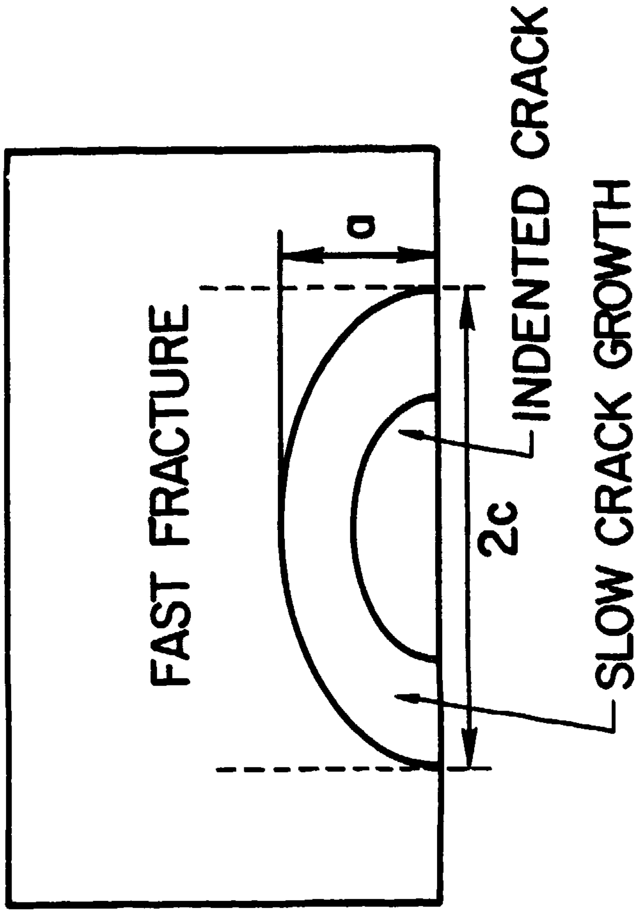

Figure 3.

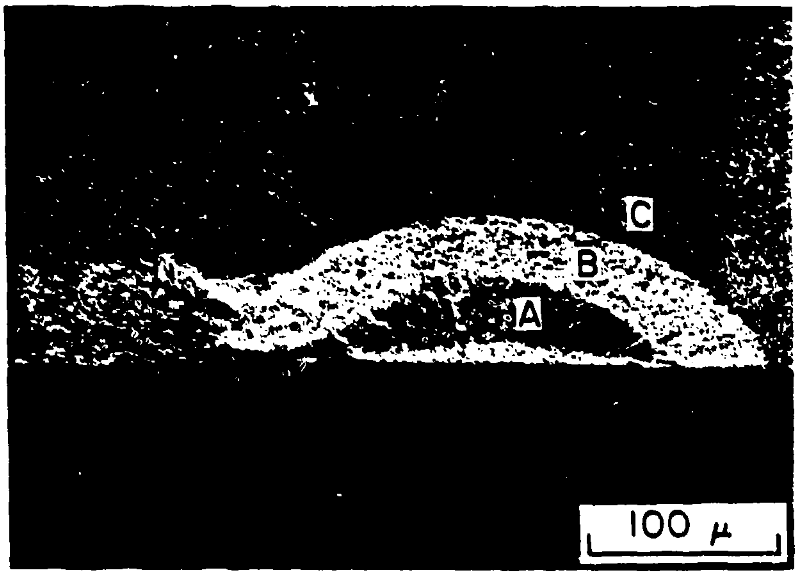

Figure 4.

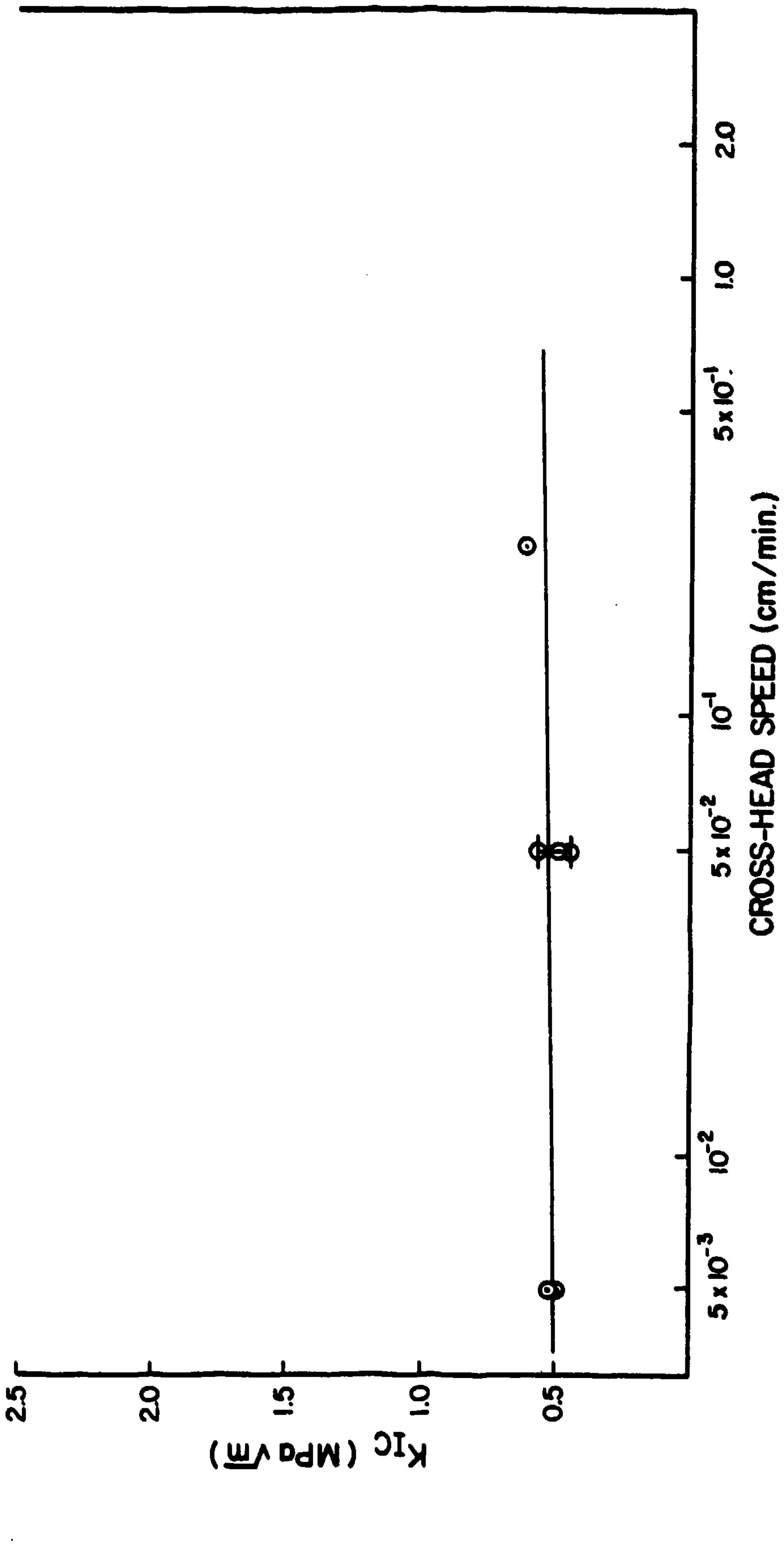

K_{IC} (MPa $\sqrt{m}$)
2.5
2.0
1.5
1.0
0.5
5 x 10⁻³
10⁻²
5 x 10⁻²
10⁻¹
5 x 10⁻¹
1.0
2.0
CROSS-HEAD SPEED (cm/min.)

Figure 5.

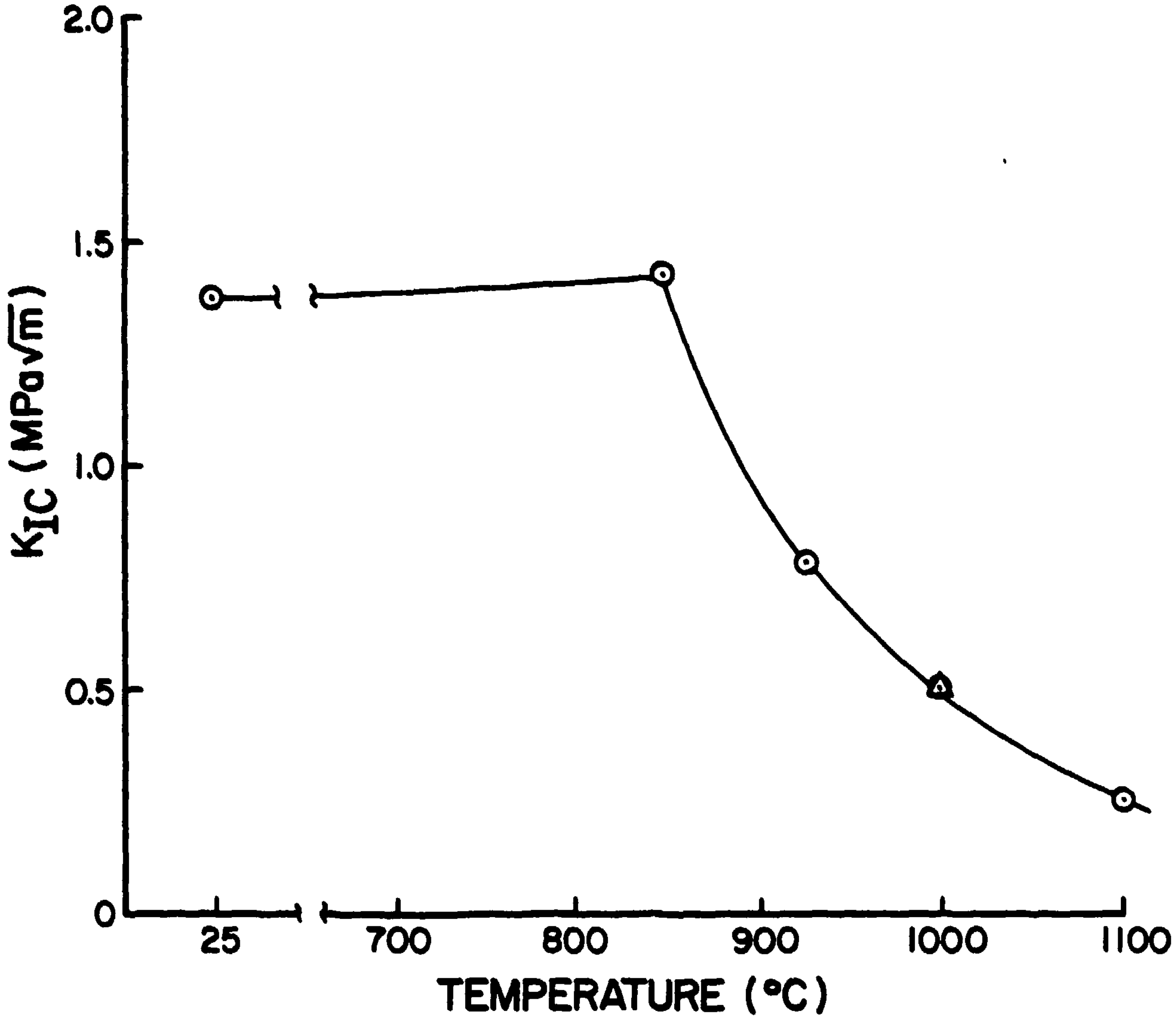
2.0
1.5
1.0
0.5
0
K_{IC} (MPa$\sqrt{m}$)
25
700
800
900
1000
1100
TEMPERATURE (°C)

Figure 6.

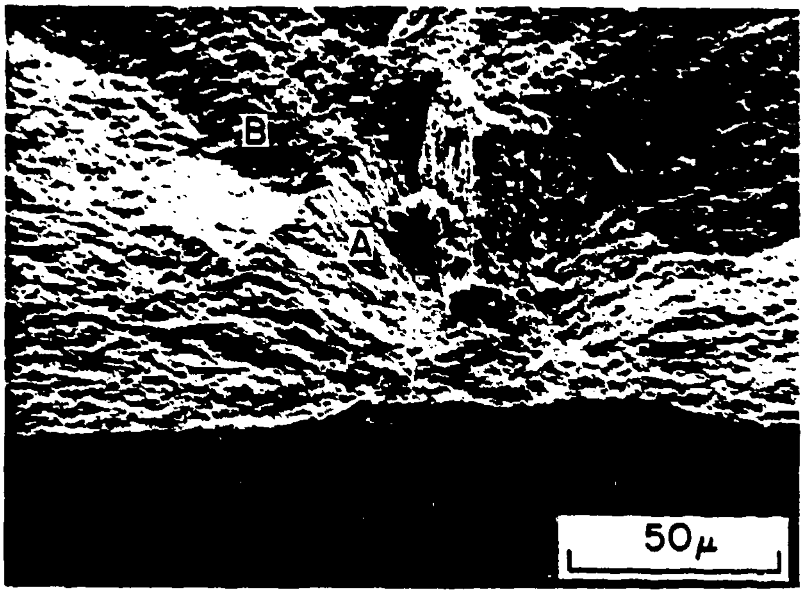

Figure 7.

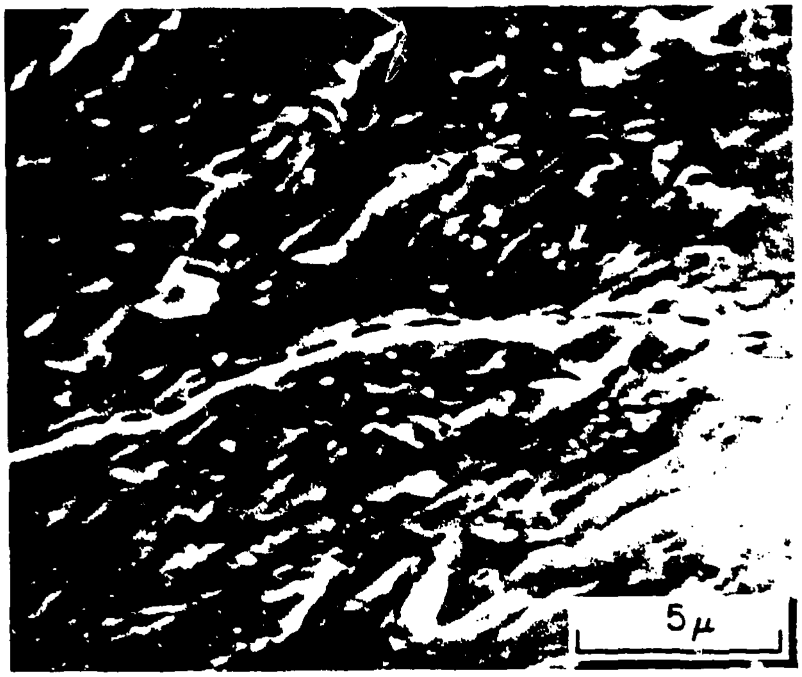

Figure 8.

Figure 9.

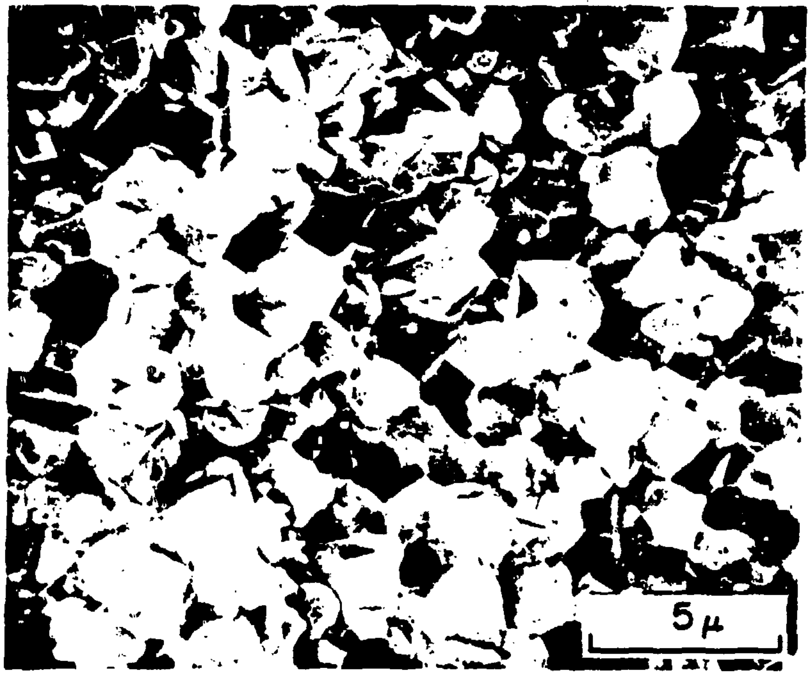

Figure 10.

Figure 11.

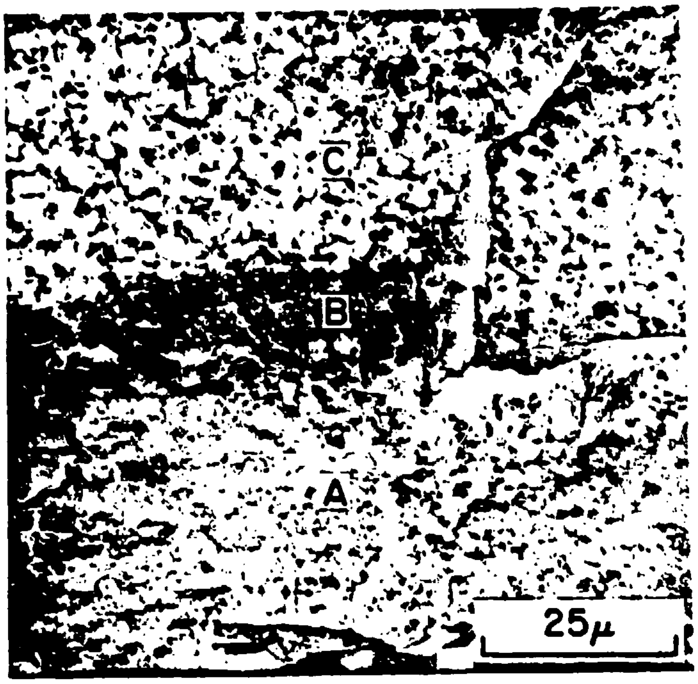

Figure 12.

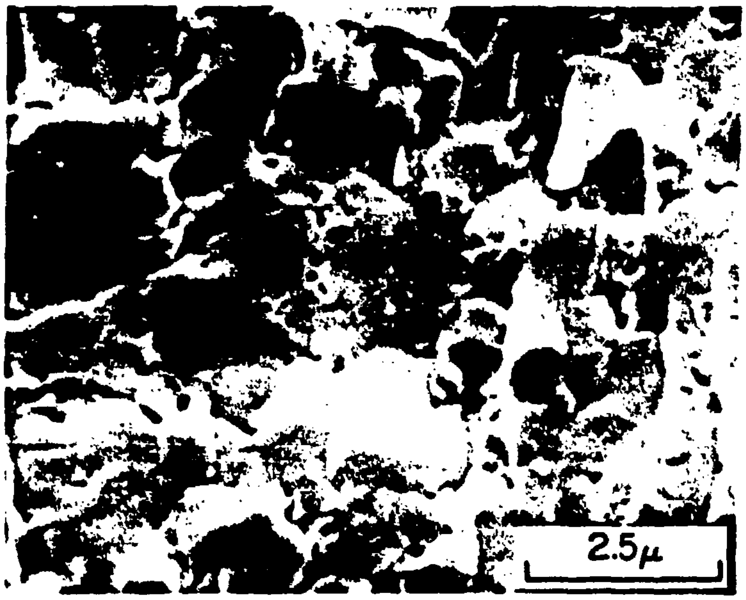

Figure 13.

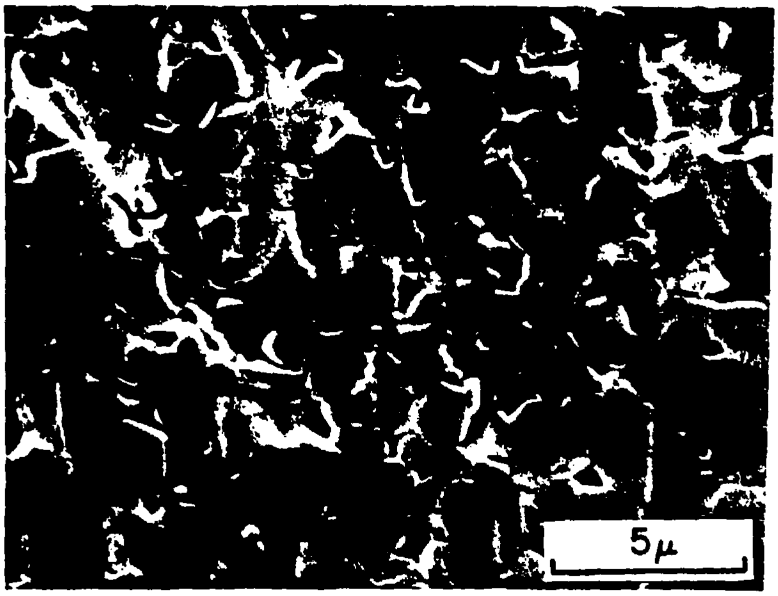

Figure 14.

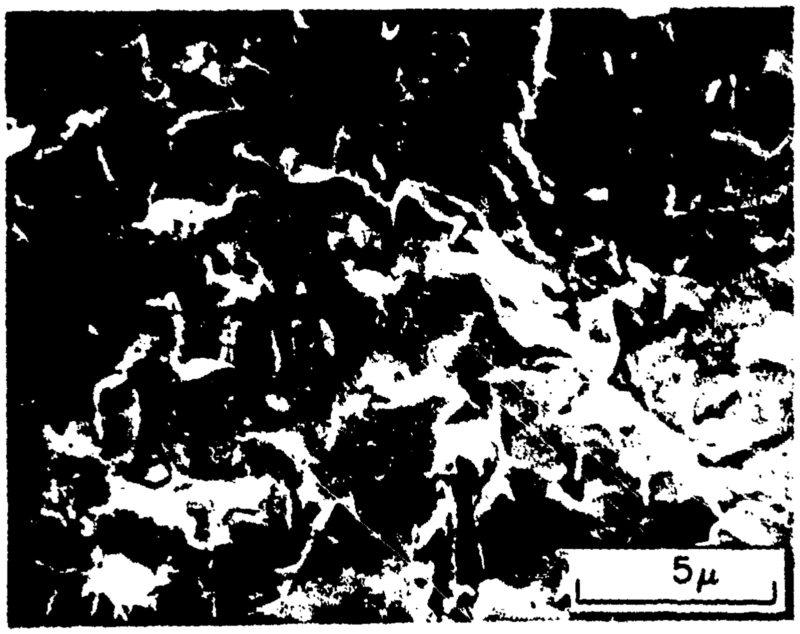

Figure 15.

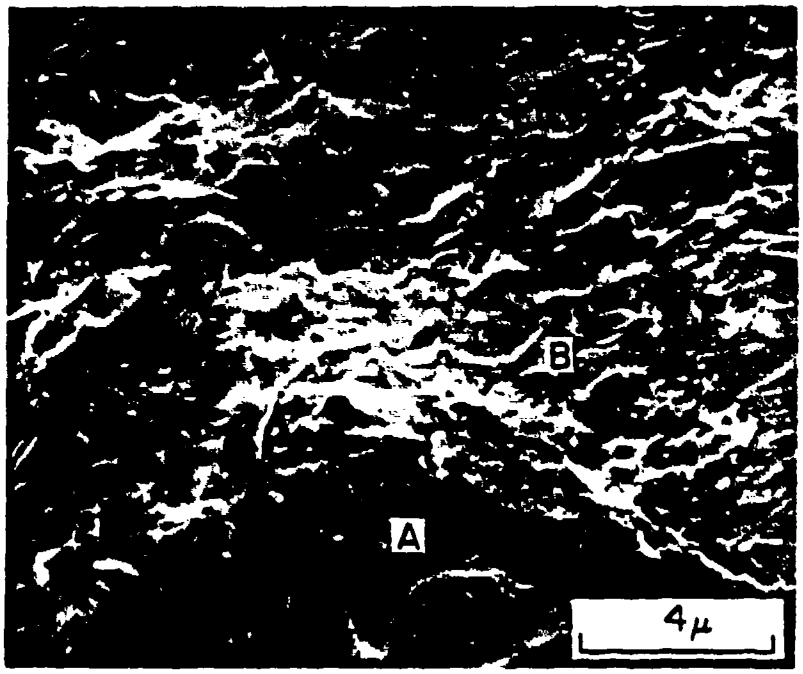

Figure 16.

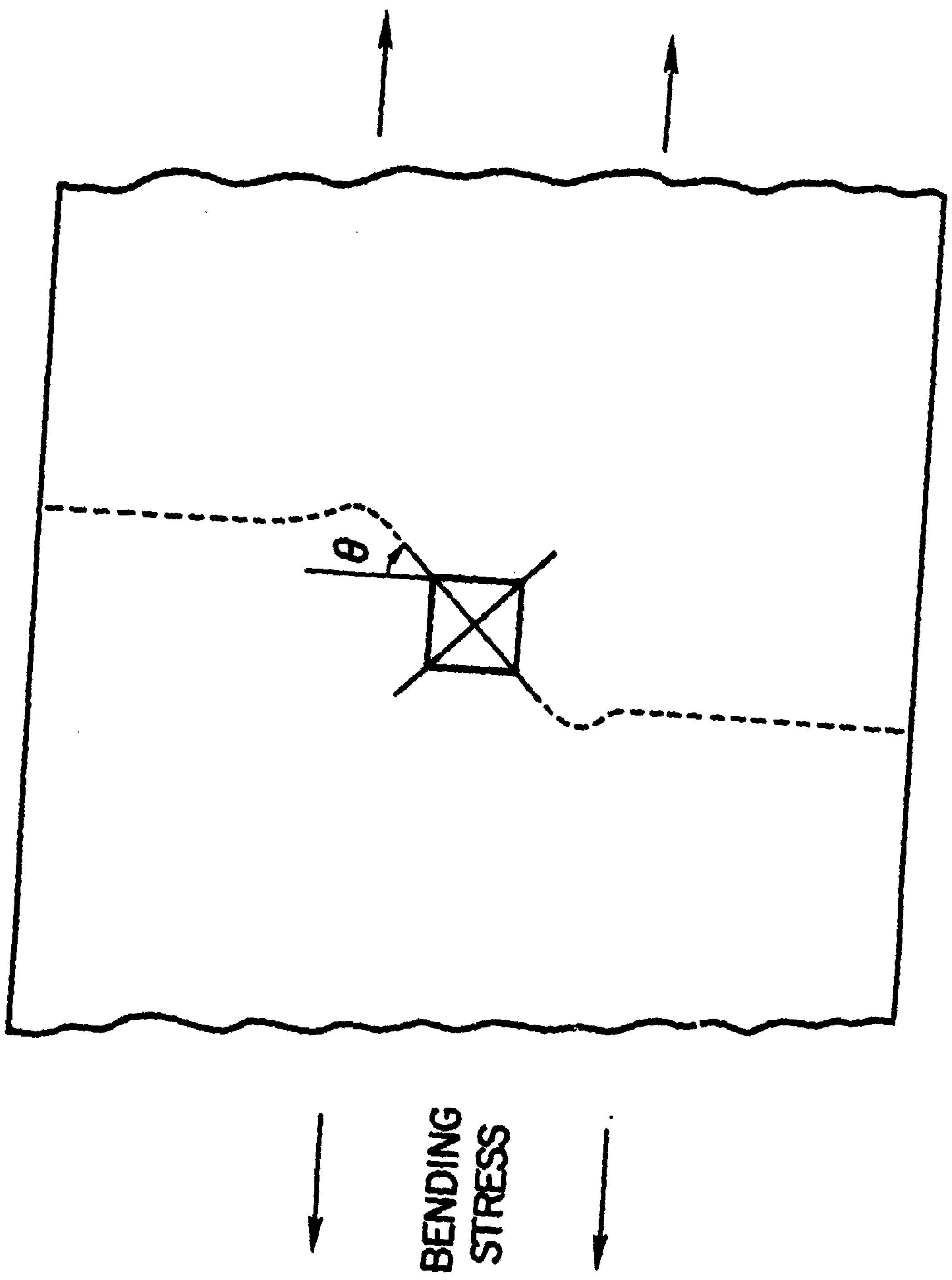

Figure 17.

Figure 18.

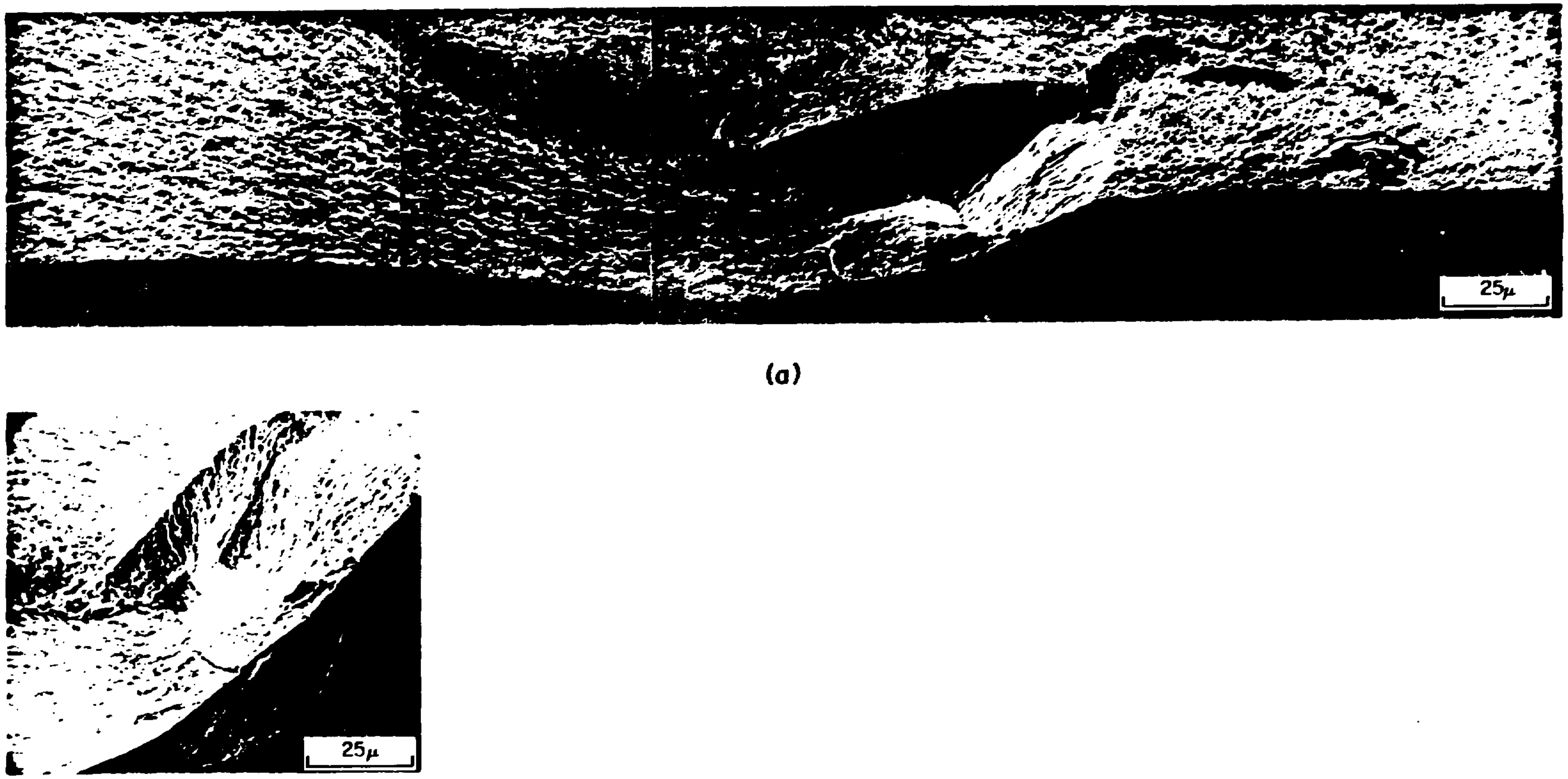

(a)

(b)